

Testing for intrinsic multifractality in the global grain spot market indices: A multifractal detrended fluctuation analysis

Li Wang^{a,b,c}, Xing-Lu Gao^a, Wei-Xing Zhou^{a,b,d,*}

^a*School of Business, East China University of Science and Technology, Shanghai 200237, China*

^b*Research Center for Econophysics, East China University of Science and Technology, Shanghai 200237, China*

^c*International Elite Engineering School, East China University of Science and Technology, Shanghai 200237, China*

^d*School of Mathematics, East China University of Science and Technology, Shanghai 200237, China*

Abstract

Grains account for more than 50% of the calories consumed by people worldwide, and military conflicts, pandemics, climate change, and soaring grain prices all have vital impacts on food security. However, the complex price behavior of the global grain spot markets has not been well understood. A recent study performed multifractal moving average analysis (MF-DMA) of the Grains & Oilseeds Index (GOI) and its sub-indices of wheat, maize, soyabeans, rice, and barley and found that only the maize and barley sub-indices exhibit an intrinsic multifractal nature with convincing evidence. Here, we utilize multifractal fluctuation analysis (MF-DFA) to investigate the same problem. Extensive statistical tests confirm the presence of intrinsic multifractality in the maize and barley sub-indices and the absence of intrinsic multifractality in the wheat and rice sub-indices. Different from the MF-DMA results, the MF-DFA results suggest that there is also intrinsic multifractality in the GOI and soyabeans sub-indices. Our comparative analysis does not provide conclusive information about the GOI and soyabeans and highlights the high complexity of the global grain spot markets.

Keywords: Econophysics, multifractal analysis, detrended fluctuation analysis, grain spot market, statistical test, IAAFT surrogates

1. Introduction

Food is a basic human need. However, food crises happened from time to time in history. The past few years have witnessed the accumulation of the ongoing food crisis, mainly driven by wars/conflicts/insecurity, the COVID-19 pandemic, weather extremes, and domestic food price inflation. António Guterres, Secretary-General of the United Nations, remarked that¹, “We are facing hunger on an unprecedented scale, food prices have never been higher, and millions of lives and livelihoods are hanging in the balance.” Grains account for more than 50% of the calories consumed by people worldwide. However, the complex behavior of the price evolution of the global grain spot markets is less researched from the perspective of complexity science, such as multifractal analysis of the grain markets.

Multifractal nature is ubiquitously present in financial time series for different financial variables [1]. Concerning agricultural assets, researchers have carried out multifractal analyses of various agricultural commodity futures in different markets [1], including returns or prices [2–6], volatility [7, 8], and trading volumes [9]. Multifractal analysis has also been performed of agricultural commodity spot markets, including returns or prices [5, 10–13] and volatility [11]. There are also studies that use joint multifractal analysis methods to investigate the relationship between two agricultural time series, including the price-volume relationships in agricultural commodity futures markets in the U.S.A. and China [9], the interest rates and commodity futures prices in the U.S.A. [4], the futures prices of the same agricultural commodities in the U.S.A. and China [8, 14], the prices of agricultural futures and spot markets in the

*Corresponding author.

Email address: wxzhou@ecust.edu.cn (Wei-Xing Zhou)

¹Forward of the 2022 *Global Report on Food Crises* (GRFC 2022), available at <https://www.fao.org/>.

U.S.A. [5], and the crude oil and agricultural futures prices [15]. All these studies reported the presence of multifractal behavior in the considered agricultural futures and in the spot prices of the considered agricultural commodities.

The multifractal behavior of several agricultural commodity spot markets is also confirmed, including the daily averaging prices of four agricultural commodities (leek, radish, onion, and Korean cabbage) in Korea [10], the daily return and volatility of four agricultural commodities (corn, soybean, oat, and wheat) in the U.S.A. [11], the monthly soybean index of the World Bank [12], the daily closing prices of five agricultural commodities (soybean, corn, wheat, soybean meal, and soybean oil) in the U.S.A. spot markets [5], and 12 agricultural commodities (ethanol, sugar, coffee, corn, cotton, rice, soybean, wheat, cattle, calf, and pork) in Brazil [13]. All these agricultural commodities are from local markets. Recently, Gao et al. performed multifractal moving average analysis (MF-DMA) of the Grains & Oilseeds Index (GOI) and its sub-indices of wheat, maize, soybeans, rice, and barley [16]. Intriguingly, through statistical tests based on surrogates generated by the iterative amplitude adjusted Fourier transform (IAAFT) algorithm, they found that the maize and barley sub-indices exhibit intrinsic multifractality, the GOI, wheat, and rice price indices do not possess multifractality, while the soybeans sub-index might have multifractal behavior [16]. The study highlights the importance of statistical tests in confirming or denying the presence of multifractal nature in real-world time series.

Indeed, performing multifractal analysis on a time series will always result in the characteristic multifractal functions $H(q)$, $\tau(q)$ and $f(\alpha)$, and they usually deviate from the theoretical results of monofractal time series. However, it does not guarantee the presence of multifractality; rather, one needs to perform statistical tests to confirm if the extracted empirical multifractality is intrinsic or not [1]. There are three sources of the empirical multifractality or apparent multifractality extracted from real time series [1], namely, the non-Gaussian distribution of the innovations (via shuffled time series, which retains the values of the original time series but destroys any linear and nonlinear correlations) [17–22], the linear long-range correlations (via the phase randomization algorithm, which retains the linear correlation but destroys the distribution and nonlinear correlations) [23–26], and the nonlinear long-range correlations [27–29]. Careful investigations based on the multifractal detrended fluctuation analysis (MF-DFA) [27–30], the wavelet transform modulus maxima (WTMM) approach [28], and the partition function approach [29] have unveiled that the key source of intrinsic multifractality in time series is the nonlinear long-range correlations, while the fat tails and/or linear correlations play a part only when nonlinear correlations are present [31].

Therefore, to statistically test the presence of intrinsic multifractality, the null model should be able to generate surrogates that are randomized copies of the original time series with the same power spectrum, which do not possess any nonlinear correlations [1]. In other words, the surrogates should preserve the values and linear long-term correlations of the original time series, but not the nonlinear correlations. In this vein, the iterated amplitude adjusted Fourier transform algorithm of Schreiber and Schmitz [32, 33] perfectly meets the requirements to generate the surrogates [1]. Indeed, this idea has been adopted and implemented in the multifractal analysis of real-world time series using the multifractal detrended fluctuation analysis [27, 34] and the multifractal detrending moving average analysis [16]. With the IAAFT surrogates, we can design statistics for $H(q)$, $\tau(q)$, $\alpha(q)$, and $f(\alpha)$ and perform statistical tests.

Different multifractal analysis methods for univariate and multivariate time series have been developed [1], such as the multifractal detrended fluctuation analysis [35], the multifractal detrending moving average analysis [36] as a generalization of the detrending moving average analysis [37, 38], the partition function approach [39–41], the structure function approach [42–44], the wavelet analysis [45], the multifractal Higuchi’s dimension analysis (MF-HDA) [46], and their variants such as the multifractal detrended fluctuation analysis based on (optimized) empirical mode decomposition [47, 48], the time-singularity multifractal spectrum distribution [49], and the extended self-similarity based multifractal detrended fluctuation analysis [50]. In this work, we will adopt the most popular method, MF-DFA, to investigate the Grains & Oilseeds Index (GOI) and its sub-indices of wheat, maize, soybeans, rice, and barley and compare with the MF-DMA results [16]. MF-DFA is the multifractal extension of the detrended fluctuation analysis (DFA), which was introduced originally to study the long-range correlations in coding and noncoding DNA nucleotide sequences [51]. We note that, although MF-DFA became the most popular method for multifractal analysis of time series in diverse fields after the work of Kantelhardt et al. [35], it was developed earlier independently by Castro e Silva and Moreira in 1997 [52] and by Weber and Talkner in 2001 [53].

In this work, we will utilize the multifractal fluctuation analysis to investigate the GOI and its sub-indices of wheat, maize, soybeans, rice, and barley by extensive statistical tests based on their IAAFT surrogates and compare with the MF-DMA results [16]. We confirm the presence of intrinsic multifractality in the maize and barley indices and the absence of intrinsic multifractality in the wheat and rice indices. Different from the MF-DMA results, the MF-DFA

results suggest that there is also intrinsic multifractality in the GOI and soyabeans indices. The partial discrepancies between the MF-DFA results and the MF-DMA results highlight the high complexity of the global grain spot markets and call for further studies on the underlying mechanisms.

The remainder of this work is organized as follows. Section 2 describes the data sets we investigate and the MF-DFA method we use. Section 3 presents the empirical results and extensive statistical tests on several characteristic multifractal variables using the IAAFT surrogate time series of the six indices. We summarize, discuss, and conclude in Section 4.

2. Data and methods

2.1. Data description

We retrieved the daily price time series of the Grains & Oilseeds Index and its five sub-indices for wheat, maize, soyabeans, rice, and barley from the International Grains Council (publicly available at <http://www.igc.int>). All six time series cover the time period from January 3, 2000 to August 31, 2022. In Fig. 1, we show the daily price time series $P(t)$ of the GOI index $P_{GOI}(t)$, the wheat sub-index $P_{Wheat}(t)$, the maize sub-index $P_{Maize}(t)$, the soyabeans sub-index $P_{Soyabeans}(t)$, the rice sub-index $P_{Rice}(t)$, and the barley sub-index $P_{Barley}(t)$. All six indices suffered from the global food crisis of 2007-2008 with sharp price rises [54–56]. The prices of wheat, maize, soyabeans, and barley also rose remarkably during 2010-2012 and 2020-2021. The recent spike in food prices is mainly caused by the ongoing COVID-19 pandemic [57–59]. In addition, Russia started the so-called “special military operation” in Ukraine since February 24, 2022 and the Russia-Ukraine crisis sparked the further rise of food prices since the two countries are the third and fourth largest exporters of agricultural products and the main exporters of fertilizers. Brokered by the United Nations and Turkey on July 22, 2022, Ukraine and Russia signed an agreement in Istanbul that would allow the resumption of vital grain exports from Ukrainian Black Sea ports, which eased the global food crisis and reversed the rising trend of food prices.

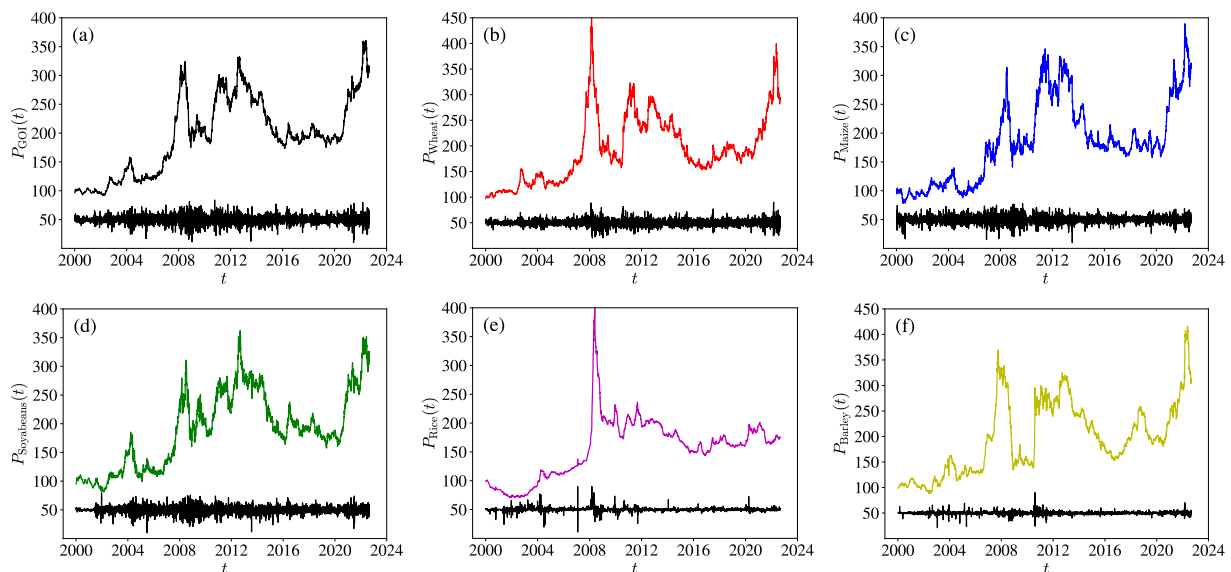


Figure 1: Daily price time series $P(t)$ and return time series $r(t)$ of the Grains & Oilseeds Index GOI (a), the wheat sub-index (b), the maize sub-index (c), the soyabeans sub-index (d), the rice sub-index (e), and the barley sub-index (f) from 3 January 2000 to 31 August 2022. Source: The official website of the International Grains Council is available at <http://www.igc.int>.

The logarithmic return $r(t)$ of each index on date t is defined as follows

$$r(t) = \ln P(t) - \ln P(t-1). \quad (1)$$

Figure 1 also shows the daily return time series $r(t)$ of the six indices. For better visibility, we manipulate $r(t)$ by stretching and vertical translation and plot the following quantity:

$$\frac{40}{\max_t(|r(t)|)} r(t) + 50. \quad (2)$$

The volatility clustering phenomenon can be observed in all return time series.

2.2. Multifractal detrended fluctuation analysis

The multifractal detrended fluctuation analysis is described briefly below.

For an index time series $P(t)$ ($t = 1, 2, \dots, N$), we first determine the polynomial trend functions $\tilde{P}_s(t)$ with respect to preset covering box sizes s [35]. For each point t , its trend value $\tilde{P}(t)$ is determined together with other points belonging to the same segment S_v based on a polynomial fitting of order ℓ to the s data points in segment S_v :

$$\tilde{P}(t) = \sum_{k=0}^{\ell} a_k t^k, \quad \ell = 1, 2, \dots. \quad (3)$$

We then detrend the index time series $P(t)$ by removing the polynomial trend function $\tilde{P}_s(i)$ from $P(t)$ as follows

$$\epsilon_s(t) = P(t) - \tilde{P}_s(t). \quad (4)$$

which results in the residual series $\epsilon_s(t)$.

We divide the residual time series $\{\epsilon_s(t)\}$ into $N_s = \text{ceil}(N/s)$ non-overlapping segments with boxes of size s , where $\text{ceil}(y)$ is the largest integer that is no larger than y . We denote the v th segment as $S_v = \{\epsilon_s((v-1)s + j) | j = 1, 2, \dots, s\}$. The local detrended fluctuation function $F_v(s)$ in the v th box is defined as the root mean square of the residuals:

$$[F_v(s)]^2 = \frac{1}{s} \sum_{i=1}^s [\epsilon_s((v-1)s + j)]^2. \quad (5)$$

The q th-order overall detrended fluctuation is

$$F_q(s) = \left\{ \frac{1}{N_s} \sum_{v=1}^{N_s} F_v^q(s) \right\}^{\frac{1}{q}}, \quad (6)$$

where q can take any real value except $q = 0$. When $q = 0$, we have

$$\ln[F_0(s)] = \frac{1}{N_s} \sum_{v=1}^{N_s} \ln[F_v(s)], \quad (7)$$

according to L'Hôpital's rule. When the whole series $\{\epsilon_s(i)\}$ cannot be completely covered by N_s boxes, one can use $2N_s$ boxes to cover the series from both ends of the series, where $N_s = \text{ceil}[N/s]$ and a short part at each end of the residuals remains uncovered [35]. We note that an alternative way is to cover the time series randomly, which is especially suitable for short time series [1, 60].

If the time series possesses fractal or multifractal nature, through varying the values of segment size s , we would obtain power-law relations between the function $F_q(s)$ and the size scale s ,

$$F_q(s) \sim s^{H(q)}. \quad (8)$$

According to the standard multifractal formalism, the multifractal scaling exponents $\tau(q)$ can also be used to characterize the multifractal properties, which reads

$$\tau(q) = qH(q) - D_f, \quad (9)$$

where D_f is the fractal dimension of the geometric support of the multifractal measure [35]. For time series, we have $D_f = 1$. If the scaling exponent function $\tau(q)$ is a nonlinear concave function of q , the investigated time series is regarded to be multifractal. We can further calculate the singularity strength function $\alpha(q)$

$$\alpha(q) = d\tau(q)/dq, \quad (10)$$

and the multifractal spectrum or singularity spectrum $f(\alpha)$

$$f(q) = q\alpha(q) - \tau(q). \quad (11)$$

All these functions characterize equivalently the multifractal nature of the time series.

In practice, it is not clear which polynomial order should be used for detrending, which may impact the results. Indeed, Oświęcimka et al. investigated several mathematical models (fractional Brownian motion, Lévy process, and binomial measure) and real-world time series and reported that the calculated singularity spectra could be very sensitive to the order of the detrending polynomial [61]. This sensitivity certainly depends on the time series under investigation. In this work, we investigated and compared the results based on the linear trend ($\ell = 1$) and the quadratic polynomial trend ($\ell = 2$). We did observe differences, which are however minor.

2.3. Generation of IAAFT surrogates

The IAAFT algorithm is implemented as follows [32, 33]. First, we obtain an initial iterated time series as a random shuffle of the original time series. Second, the Fourier spectra of the original time series and the iterated time series are calculated. Third, the squared coefficients of the iterated time series are replaced by those of the original time series, while the phases remain unchanged. Fourth, the amplitudes of the generated time series are replaced by the values of the original sorted list with the same ranking. The last four steps iterate until the preset convergence condition is satisfied.

3. Empirical analysis

In this section, we perform multifractal detrended fluctuation analysis of each index time series. To investigate the possible impact of the choice of trend functions, we adopt the first-order ($\ell = 1$) and second-order ($\ell = 2$) polynomials to detrend the index price time series. We find that the results are almost the same qualitatively, with only slight differences. Hence, we show below the results based on the linear trend function in many places and all the comparative results when necessary. There are three issues we need to clarify:

- (1) Determine the range of q . Since higher-order moments in multifractal analysis diverge for large q 's [62, 63], we use $q \in [-5, 5]$ in our analysis, which also makes our MF-DFA results comparable to the MF-DMA results in Ref. [16].
- (2) Determine the scaling range. Kantelhardt et al. suggested to perform multifractal analysis in the scaling range $s \in [10, N/4]$ [35]. In the MF-DMA analysis of GOI indices, Gao et al. used $s \in [10, 10^{2.5}] = [10, 316]$ [16], which is consistent with Ref. [35] and slightly wider than the average width of scaling ranges in many practical studies [64, 65]. In this work, we use $s \in [20, 10^{2.5}] = [20, 316]$, which is a little bit narrower. The reason is that, for smaller scales s , there are very large residuals which result in very small negative-order moments such that $F_q(s) \rightarrow 0$. In this sense, MF-DMA performs better than MF-DFA.
- (3) Generate surrogates. To perform statistical tests, we generate 1000 IAAFT surrogates for each index time series. We also find that, in several situations, about 100 surrogates can already provide decisive results.

3.1. Scaling plots

Fig. 2 illustrates the scaling plots of the MF-DFA fluctuation functions $F_q(s)$ with respect to the scale s for $q = -5, -2, 0, 2, \text{ and } 5$. It can be observed that all the lines show evident power laws, except for soyabeans when q is negative, where the scaling range should be narrower. Nevertheless, for comparability, we use the same scaling range for all q values and all indices. In addition, we find that the scaling behavior is better for positive orders ($q > 0$) than

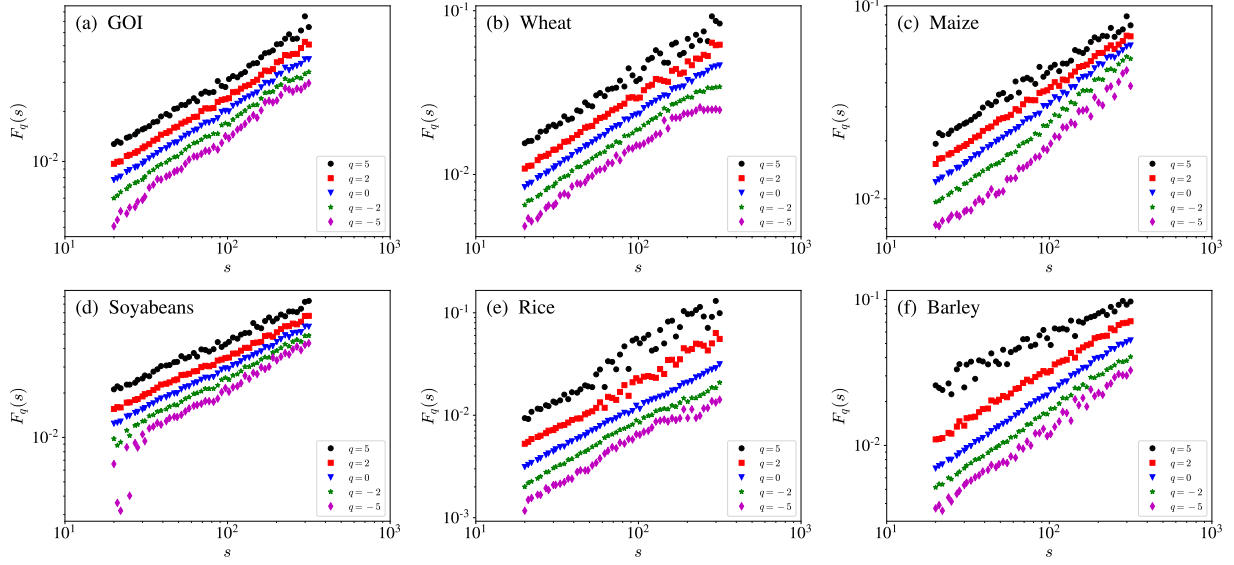


Figure 2: Scaling plots of the MF-DFA fluctuation function $F_q(s)$ with respect to the scale s for the GOI index (a), the wheat sub-index (b), the maize sub-index (c), the soyabeans sub-index (d), the rice sub-index (e), and the barley sub-index (f). The polynomial used to detrend the indices is a linear function with $\ell = 1$.

for negative orders ($q < 0$). There may also be log-periodic oscillations around the power law [66], suggesting the possible presence of multiplicative cascades among different scales with a characteristic discrete scale ratio.

The scaling plots look similar when we detrend the indices with quadratic polynomials ($\ell = 2$), as shown in Fig. A1. For instance, for negative q the two $F_q(s)$ functions for $\ell = 1$ and $\ell = 2$ deviate remarkably when s is small, and the deviation becomes larger when $|q|$ is larger.

3.2. Generalized Hurst indexes

We perform linear regression of $\ln F_q(s)$ against $\ln s$ for different values of q to estimate the generalized Hurst indexes $H(q)$ of the six global grain spot price indices. For each GOI and sub-indices, we generate 1000 IAAFT surrogate time series and calculate the $\hat{H}(q)$ function for each surrogate to obtain the mean $\langle \hat{H}(q) \rangle$ and standard deviation $\sigma_{\hat{H}}$. The results for $\ell = 1$ are illustrated in Fig. 3. The results for $\ell = 2$ are similar, which are shown in Fig. A2. For GOI in Fig. 3(a) and Soyabeans in Fig. 3(d), the $q > 0$ part of $H(q)$ falls within the confidence interval such that $\langle \hat{H}(q) \rangle - \sigma_{\hat{H}} < H(q) < \langle \hat{H}(q) \rangle + \sigma_{\hat{H}}$, while the $q < 0$ part of $H(q)$ is above the confidence interval such that $H(q) > \langle \hat{H}(q) \rangle + \sigma_{\hat{H}}$. For wheat in Fig. 3(b), the $q > 2$ part of $H(q)$ falls within the confidence interval such that $\langle \hat{H}(q) \rangle - \sigma_{\hat{H}} < H(q) < \langle \hat{H}(q) \rangle + \sigma_{\hat{H}}$, while the $q < 2$ part of $H(q)$ is below the confidence interval such that $H(q) < \langle \hat{H}(q) \rangle - \sigma_{\hat{H}}$. In contrast, when $\ell = 2$, $\langle \hat{H}(q) \rangle - \sigma_{\hat{H}} < H(q) < \langle \hat{H}(q) \rangle + \sigma_{\hat{H}}$ for all q values. For maize in Fig. 3(c), we find that $H(q) < \langle \hat{H}(q) \rangle - \sigma_{\hat{H}}$ when $q > 2$ and $H(q) > \langle \hat{H}(q) \rangle + \sigma_{\hat{H}}$ when $q < 2$. For rice in Fig. 3(e), we find that $H(q) < \langle \hat{H}(q) \rangle - \sigma_{\hat{H}}$ when $q < 2$ and $H(q) > \langle \hat{H}(q) \rangle + \sigma_{\hat{H}}$ when $q > 2$. For barley in Fig. 3(f), we find that $\langle \hat{H}(q) \rangle - \sigma_{\hat{H}} < H(q) < \langle \hat{H}(q) \rangle + \sigma_{\hat{H}}$ when $q < 2$ and $H(q) < \langle \hat{H}(q) \rangle + \sigma_{\hat{H}}$ when $q > 2$. All the $H(q)$ curves deviate from the confidence intervals (shadow areas) $\langle \hat{H}(q) \rangle \pm \sigma_{\hat{H}}$, indicating that the complex behavior of the global grain spot price indices cannot be attributed only to the fat-tailed distributions and the linear correlations. However, the $H(q)$ curves of wheat and rice are not monotonically decreasing functions, showing that there is no multifractal nature or the multifractal nature has been ‘‘contaminated’’.

One common feature of the six plots in Fig. 3 is that all the Hurst indexes $H(2)$ fall well within the confidence intervals:

$$\langle \hat{H}(q) \rangle - \sigma_{\hat{H}} < H(2) < \langle \hat{H}(q) \rangle + \sigma_{\hat{H}} \quad (12)$$

and $\sigma_{\hat{H}(2)}$ is the smallest among all $\sigma_{\hat{H}(q)}$, which confirms the validation of the IAAFT method in generating required surrogates and the MF-DFA approach in determining the Hurst indexes since the surrogates has the power spectra as

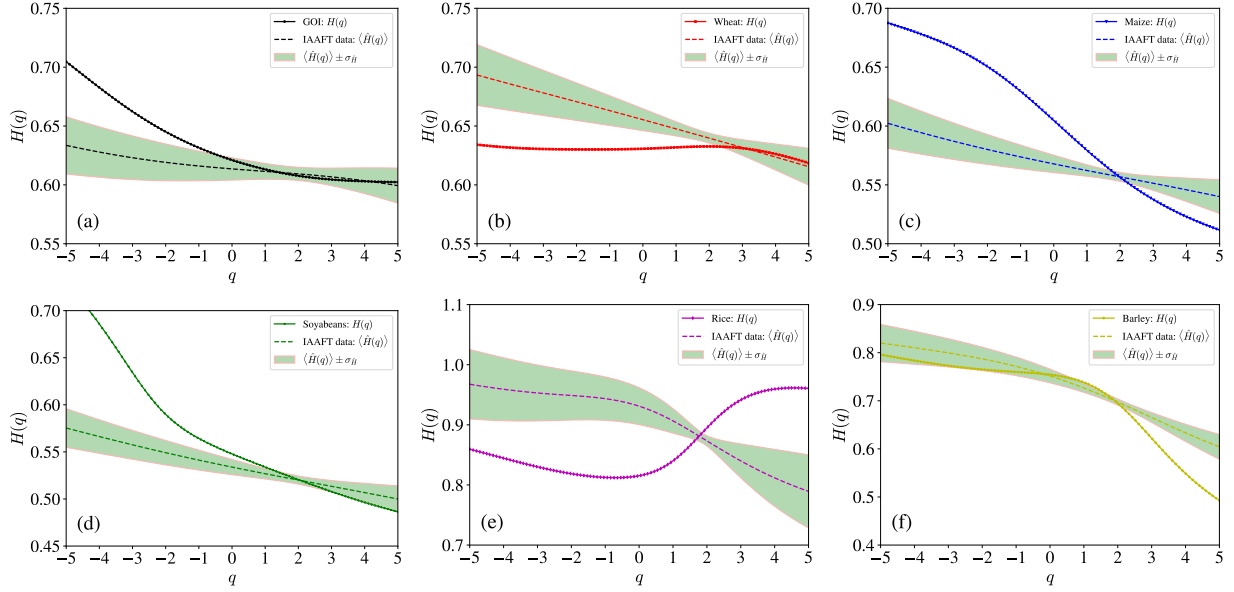


Figure 3: Generalized Hurst indexes $H(q)$ with respect to the order q for the GOI index (a), the wheat sub-index (b), the maize sub-index (c), the soyabeans sub-index (d), the rice sub-index (e), and the barley sub-index (f). The polynomial used to detrend the indices is a linear function with $\ell = 1$. For each GOI and sub-indices, we generate 1000 surrogate time series using the IAAFT algorithm and calculate the mean $\langle \hat{H} \rangle$ and standard deviation $\sigma_{\hat{H}}$.

the original time series. Indeed, Fig. 2 shows that the $\log F_2(s) \sim \log s$ curves are nice straight lines. In Table 1, we present the Hurst indexes of the six time series obtained using MF-DMA, MF-DFA ($\ell = 1$) and MF-DFA ($\ell = 2$). For each time series, the Hurst indexes estimated from three methods are close to each other. Specifically, only the Hurst indexes for maize and soyabeans are close to 0.5, while the Hurst indexes for GOI, wheat, and barley are greater than 0.6 and that for rice is greater than 0.7. It shows that the global rice spot price index has strong linear long-term correlations, and the global spot price indices of GOI, wheat, and barley also contain linear long-term correlations.

Table 1: Hurst indexes $H(2)$ of the six global grain spot price indices estimated using MF-DMA, MF-DFA ($\ell = 1$) and MF-DFA ($\ell = 2$).

Method	GOI	Wheat	Maize	Soyabeans	Rice	Barley
MF-DMA	0.6280	0.6239	0.5373	0.5355	0.7255	0.6448
MF-DFA ($\ell = 1$)	0.6080	0.6327	0.5579	0.5214	0.8908	0.6989
MF-DFA ($\ell = 2$)	0.5846	0.6437	0.5540	0.5138	0.8271	0.7113

3.3. Mass exponents

According to Eq. (9), the mass exponents $\tau(q)$ can be calculated numerically from the generalized Hurst indexes $H(q)$. We calculate the deviation of the mass exponents $\tau(q)$ of the original time series from the average mass exponents $\langle \hat{\tau}(q) \rangle$ of the IAAFT surrogates, denoted as $\tau(q) - \langle \hat{\tau}(q) \rangle$. Fig. 4 shows $\tau(q) - \langle \hat{\tau}(q) \rangle$ as a function of the order q for the six indices. We find that all the $\tau(q)$ curves deviate from the confidence level. For GOI in Fig. 4(a) and soyabeans in Fig. 4(d), $\tau(q) < \langle \hat{\tau}(q) \rangle - \sigma_{\hat{\tau}}$ when $q < -1$ and $\langle \hat{\tau}(q) \rangle - \sigma_{\hat{\tau}} < \tau(q) < \langle \hat{\tau}(q) \rangle + \sigma_{\hat{\tau}}$ when $q > -1$. For wheat in Fig. 4(b), $\tau(q) > \langle \hat{\tau}(q) \rangle + \sigma_{\hat{\tau}}$ when $q < 0$ and $\langle \hat{\tau}(q) \rangle - \sigma_{\hat{\tau}} < \tau(q) < \langle \hat{\tau}(q) \rangle + \sigma_{\hat{\tau}}$ when $q \geq 0$. However, when $\ell = 2$, Fig. A3(d') shows that $\tau(q)$ falls within the confidence interval for all q values. For maize in Fig. 4(c), $\tau(q) < \langle \hat{\tau}(q) \rangle - \sigma_{\hat{\tau}}$ when $q < 0$ and $q > 2$. For rice in Fig. 4(e), $\tau(q) > \langle \hat{\tau}(q) \rangle + \sigma_{\hat{\tau}}$ when $q < 0$ and $q > 2$ and $\tau(q) < \langle \hat{\tau}(q) \rangle - \sigma_{\hat{\tau}}$ when $0 \leq q \leq 2$. For barley in Fig. 4(f), $\langle \hat{\tau}(q) \rangle - \sigma_{\hat{\tau}} < \tau(q) < \langle \hat{\tau}(q) \rangle + \sigma_{\hat{\tau}}$ when $q \leq 2$ and $\tau(q) < \langle \hat{\tau}(q) \rangle - \sigma_{\hat{\tau}}$ when $q > 2$. In all the six plots, we find that $\tau(0) = \langle \hat{\tau}(0) \rangle$ and $\tau(2) \approx \langle \hat{\tau}(2) \rangle$, and $\sigma_{\hat{\tau}(0)} = 0$ and $\sigma_{\hat{\tau}(2)} \approx 0$.

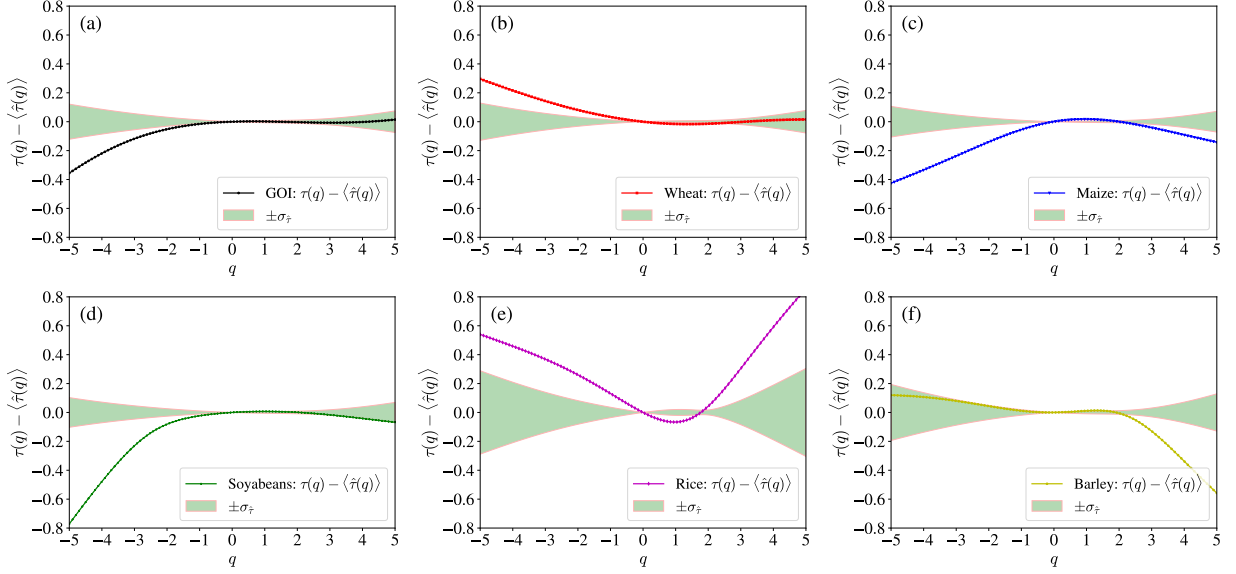


Figure 4: Deviations $(\tau(q) - \langle \hat{\tau}(q) \rangle)$ of the mass exponents $\tau(q)$ of the original time series from the average mass exponents $\langle \hat{\tau}(q) \rangle$ of the IAAFT surrogates with respect to the order q for the GOI index (a), the wheat sub-index (b), the maize sub-index (c), the soyabeans sub-index (d), the rice sub-index (e), and the barley sub-index (f). The polynomial used to detrend the indices is a linear function with $\ell = 1$. For each GOI and sub-indices, we generate 1000 surrogate time series using the IAAFT algorithm and calculate the mean $\langle \hat{\tau} \rangle$ and standard deviation $\sigma_{\hat{\tau}}$.

Table 2: Testing the nonlinearities of the mass exponent function $\tau(q)$ of the six indices. The mass exponent function is assumed to have a quadratic form $\tau(q) = a_0 + a_1q + a_2q^2$. We test if $a_2 = 0$ or not. The upper panel is for $\ell = 1$, while the lower panel is for $\ell = 2$.

Index	Full model			Linear term			Quadratic term		
	F -stat	p -value	R^2	a_1	t -stat	p -value	a_2	t -stat	p -value
GOI	270026	0.0000	0.9998	0.6415	734	0.0000	-0.0102	-30	0.0000
Wheat	3347494	0.0000	1.0000	0.6290	2587	0.0000	-0.0013	-13	0.0000
Maize	990196	0.0000	1.0000	0.6009	1402	0.0000	-0.0180	-109	0.0000
Soyabeans	56755	0.0000	0.9991	0.5869	334	0.0000	-0.0247	-36	0.0000
Rice	92753	0.0000	0.9995	0.8948	430	0.0000	0.0118	14	0.0000
Barley	28042	0.0000	0.9982	0.6749	235	0.0000	-0.0311	-28	0.0000
GOI	206749	0.0000	0.9998	0.6401	641	0.0000	-0.0185	-48	0.0000
Wheat	3005762	0.0000	1.0000	0.6566	2450	0.0000	-0.0095	-92	0.0000
Maize	1466824	0.0000	1.0000	0.5874	1709	0.0000	-0.0144	-108	0.0000
Soyabeans	21590	0.0000	0.9977	0.6319	205	0.0000	-0.0391	-33	0.0000
Rice	143795	0.0000	0.9997	0.8717	536	0.0000	-0.0046	-7	0.0000
Barley	39694	0.0000	0.9988	0.6933	279	0.0000	-0.0355	-37	0.0000

For multifractal time series, the mass exponent function is nonlinear. To test the nonlinearity of the $\tau(q)$ function, we assume that that [1]

$$\tau(q) = a_0 + a_1q + a_2q^2. \quad (13)$$

We test if $a_2 \neq 0$ by regressing the the mass exponents $\tau(q)$ to Eq. (13). The regression results are shown in Table 2. The upper panel is for $\ell = 1$, while the lower panel is for $\ell = 2$. For the full model, we have p -values close to 0 and the R^2 close to 1, indicating that the model fits the data very well. The coefficients a_2 of the quadratic term are significantly different from 0 with close-to-zero p -values for all the time series. However, we find that $a_2 > 0$ for rice when $\ell = 1$. There are some differences when MF-DMA is adopted [16], where a_2 for wheat is insignificantly different from 0 with the p -value being 0.2694 and $a_2 > 0$ for GOI and wheat.

3.4. Singularity spectrum

3.4.1. Empirical singularity spectrum

For each GOI and sub-indices, the singularity exponents $\alpha(q)$ and the singularity spectrum $f(q)$ can be numerically calculated using Eq. (10) and Eq. (11). For each index, we generate 1000 surrogate time series using the IAAFT algorithm and calculate the mean $\langle \hat{f} \rangle(\alpha)$ and standard deviation $\sigma_{\hat{f}}$. The resulting multifractal singularity spectra are shown in Fig. 5.

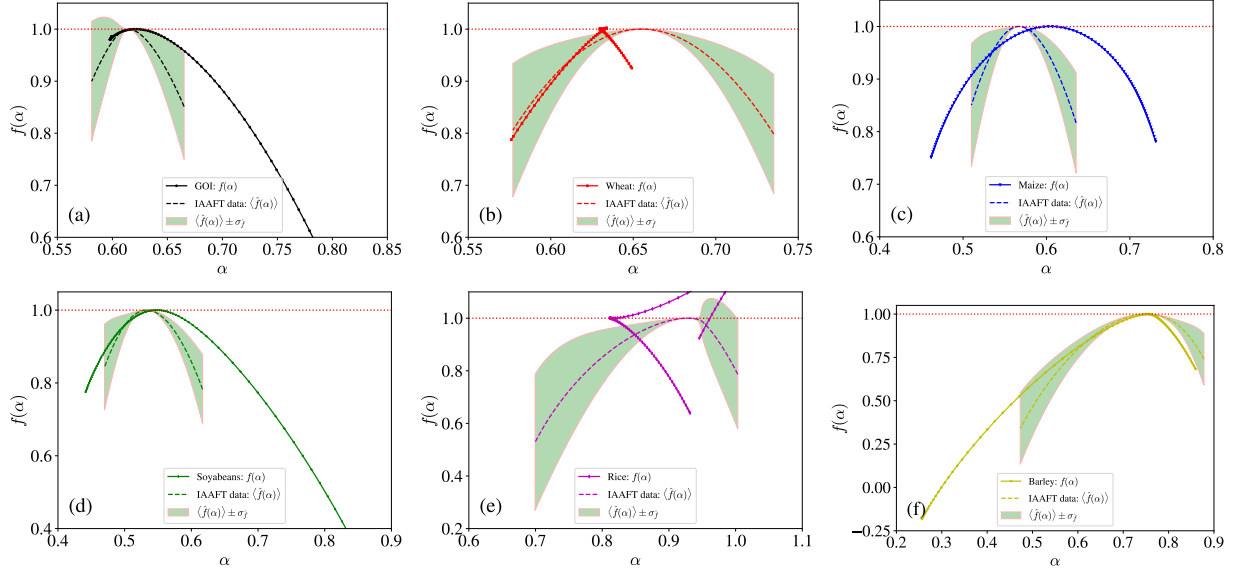


Figure 5: Singularity spectrum $f(\alpha)$ with respect to the singularity α for the GOI index (a), the wheat sub-index (b), the maize sub-index (c), the soybeans sub-index (d), the rice sub-index (e), and the barley sub-index (f). The polynomial used to detrend the indices is a linear function with $\ell = 1$. For each GOI and sub-indices, we generate 1000 surrogate time series using the IAAFT algorithm and calculate the mean $\langle \hat{f} \rangle(\alpha)$ and standard deviation $\sigma_{\hat{f}}$.

We find that all the the mean multifractal singularity spectra $\langle \hat{f} \rangle(\alpha)$ of the IAAFT surrogates have a nice bell-like shape as the singularity spectra of classic mathematical models [1]. Moreover, their singularity widths $\Delta \hat{\alpha}$ are significantly greater than 0, which highlights the potential power of the broad return distribution and possible linear long-term correlations to generate illusionary multifractality for multifractality-free IAAFT surrogates. For GOI, maize, soyabeans and barley, the singularity spectra $f(\alpha)$ are also bell-shaped, and their singularity $\Delta \alpha$ widths are significantly greater than those of the null models $\langle \Delta \hat{\alpha} \rangle$,

$$\Delta \alpha > \langle \Delta \hat{\alpha} \rangle. \quad (14)$$

In contrast, for wheat and rice, we have

$$\Delta \alpha < \langle \Delta \hat{\alpha} \rangle, \quad (15)$$

and $\Delta \alpha < 0$ for rice. The singularity spectra of wheat and rice have a knot. The results obtained from MF-DFA with $\ell = 2$ are very similar, as shown in Fig. A5, except for wheat whose singularity spectrum becomes bell-shaped and the singularity width is significantly greater than the IAAFT surrogates.

3.4.2. Statistical tests based on Singularity width

The strength of multifractality is one of the most important quantities of multifractal time series, which is characterized by the singularity width

$$\Delta \alpha = \alpha(-\infty) - \alpha(+\infty) \triangleq \alpha_{\max} - \alpha_{\min} \quad (16)$$

where α_{\max} and α_{\min} are not the asymptotic values for $q = \pm \infty$ but for $q = 5$ in our empirical analysis [1]. In practice, we try to test if $\Delta \alpha$ is greater than $\Delta \hat{\alpha}$ of the IAAFT surrogates [16]. Speaking differently, we need to calculate the

probability that $\Delta\alpha$ is greater than $\Delta\hat{\alpha}$:

$$p\text{-value} = \Pr(\Delta\alpha < \Delta\hat{\alpha}). \quad (17)$$

If the p -value is smaller than a preset significance level, say 5%, we reject the hypothesis that the original time series is monofractal. Otherwise, the original time series cannot be distinguished from the IAAFT surrogates which contain only linear correlations.

For each spot price index, we generate 1000 IAAFT surrogates and determine their singularity widths $\Delta\hat{\alpha}$. The empirical distributions of singularity widths $\Delta\hat{\alpha}$ of the six spot price indices are illustrated in Fig. 6. We find that wheat in Fig. 6(b) and rice in Fig. 6(e) have large p -values, while the rest four spot price indices have very small p -values. As shown in Fig. A6, the results obtained from MF-DFA with $\ell = 2$ are qualitatively the same, except for wheat whose p -value becomes much smaller.

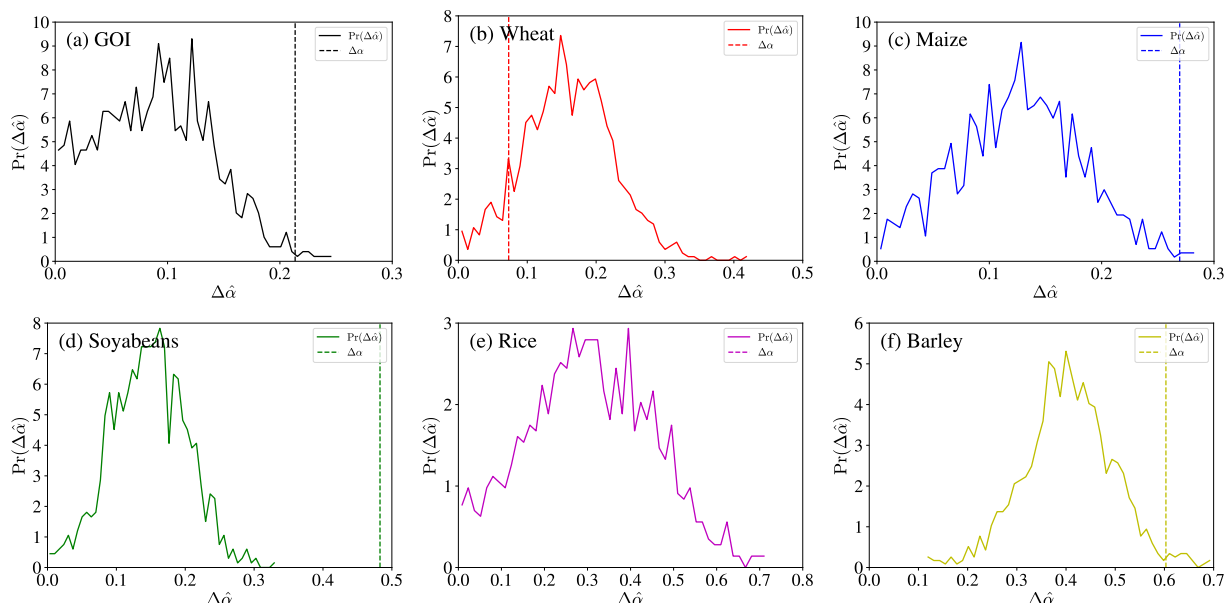


Figure 6: Empirical distribution of the singularity widths $\Delta\hat{\alpha}$ of the 1000 IAAFT surrogates for the GOI index (a), the wheat sub-index (b), the maize sub-index (c), the soyabeans sub-index (d), the rice sub-index (e), and the barley sub-index (f). The polynomial used to detrend the indices is a linear function with $\ell = 1$. The vertical dashed lines are the corresponding singularity widths $\Delta\alpha$ of the original time series. Note that $\Delta\alpha < 0$ for rice, which is not shown in plot (e).

Table 3: Testing multifractality based on singularity width. Here, $\Delta\alpha$ is the singularity width of the original time series, $\langle\Delta\hat{\alpha}\rangle$ is the average singularity width of the 1000 IAAFT surrogates, $\sigma_{\Delta\hat{\alpha}}$ is the standard deviation of the singularity widths of the 1000 IAAFT surrogates, and p -value is the proportion of IAAFT surrogates with $\Delta\hat{\alpha} > \Delta\alpha$.

Index	MF-DFA with $\ell = 1$				MF-DFA with $\ell = 2$			
	$\Delta\alpha$	$\langle\Delta\hat{\alpha}\rangle$	$\sigma_{\Delta\hat{\alpha}}$	p -value	$\Delta\alpha$	$\langle\Delta\hat{\alpha}\rangle$	$\sigma_{\Delta\hat{\alpha}}$	p -value
GOI	0.2136	0.0891	0.0502	0.0090	0.3361	0.1140	0.0468	0.0000
Wheat	0.0730	0.1594	0.0649	0.9040	0.2385	0.1513	0.0572	0.0640
Maize	0.2695	0.1266	0.0560	0.0040	0.2124	0.1286	0.0463	0.0310
Soyabeans	0.4828	0.1474	0.0545	0.0000	0.7253	0.1682	0.0458	0.0000
Rice	-0.0139	0.3060	0.1442	1.0000	0.1494	0.3546	0.1304	0.9320
Barley	0.6030	0.4050	0.0910	0.0200	0.7183	0.4141	0.0817	0.0010

For each global grain spot price index, We calculate the singularity width $\delta\alpha$, the average singularity width $\langle\Delta\hat{\alpha}\rangle$ of the 1000 IAAFT surrogates, the standard deviation of the singularity widths $\sigma_{\Delta\hat{\alpha}}$ of the 1000 IAAFT surrogates,

and the p -value that $\delta\alpha$ is smaller than $\Delta\hat{\alpha}$. These characteristic values are presented in Table 3 for $\ell = 1$ and $\ell = 2$. It shows that rice and barley have much larger $\sigma_{\Delta\hat{\alpha}}$ values, quantifying the broader distributions in Fig. 6(e,f). For GOI, maize, soyabeans, and barley, $\langle\Delta\hat{\alpha}\rangle < \Delta\alpha$ and their p -values are very small, suggesting that these time series may have an intrinsic multifractal nature that cannot be explained by the fat-tailedness of returns and possible long-term linear correlations in returns. In contrast, for wheat and rice, the p -values are large, which indicates the absence of intrinsic multifractality.

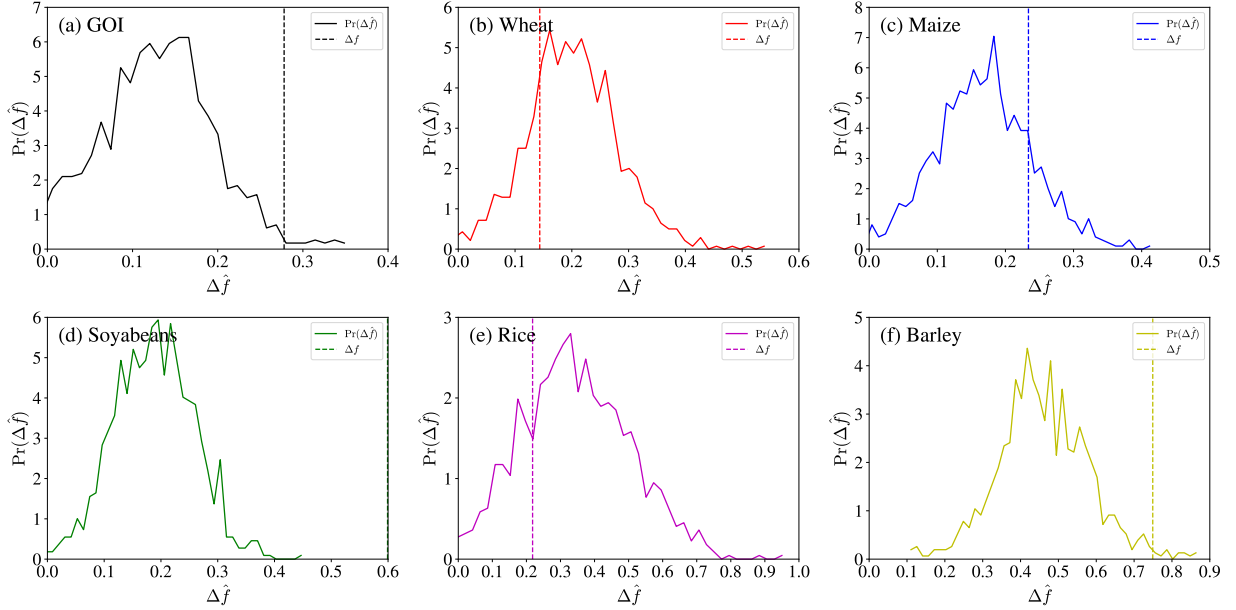


Figure 7: Empirical distribution of the spectrum differences $\Delta\hat{f}$ of the 1000 IAAFT surrogates for the GOI index (a), the wheat sub-index (b), the maize sub-index (c), the soyabeans sub-index (d), the rice sub-index (e), and the barley sub-index (f). The polynomial used to detrend the indices is a linear function with $\ell = 1$. The vertical dashed lines are the corresponding spectrum differences Δf of the original time series.

3.4.3. Statistical tests based on spectrum difference

Following Refs. [16, 67, 68], we next perform statistical tests based on the spectrum difference Δf , which is defined as follows,

$$\Delta f = 1 - [f(\alpha_{\min}) + f(\alpha_{\max})]/2. \quad (18)$$

We aim to test if Δf is significantly greater than $\Delta\hat{f}$ of the IAAFT surrogates [16]. Speaking differently, we calculate the probability that Δf is greater than $\Delta\hat{f}$:

$$p\text{-value} = \Pr(\Delta f < \Delta\hat{f}). \quad (19)$$

We note that, this test alone is not capable of rejecting multifractality; Rather, it is used to confirm the conclusion of the statistical tests based on singularity width.

For each spot price index, we generate 1000 IAAFT surrogates and determine their spectrum differences $\Delta\hat{f}$. The empirical distributions of spectrum differences $\Delta\hat{f}$ of the six spot price indices are illustrated in Fig. 7. We find that wheat in Fig. 7(b), maize in Fig. 7(c) and rice in Fig. 7(e) have large p -values, while the rest three spot price indices have very small p -values. As shown in Fig. A7, the results obtained from MF-DFA with $\ell = 2$ are qualitatively the same, except again for wheat whose p -value becomes much smaller.

For each global grain spot price index, we calculate the spectrum difference δf , the average spectrum difference $\langle\Delta\hat{f}\rangle$ of the 1000 IAAFT surrogates, the standard deviation of spectrum differences $\sigma_{\Delta\hat{f}}$ of the 1000 IAAFT surrogates, and the p -value that δf is smaller than $\Delta\hat{f}$. These characteristic values are presented in Table 4 for $\ell = 1$ and $\ell = 2$.

The large p -values for wheat and maize echo the results for $\Delta\alpha$ in Table 3. However, the large p -value for maize does not deny the conclusion extracted from Table 3.

Table 4: Testing multifractality based on singularity spectrum difference Δf . Here, Δf is the spectrum difference of the original time series, $\langle\Delta\hat{f}\rangle$ is the average spectrum difference of the 1000 IAAFT surrogates, $\sigma_{\Delta\hat{f}}$ is the standard deviation of the spectrum differences of the 1000 IAAFT surrogates, and p -value is the proportion of IAAFT surrogates with $\Delta\hat{f} > \Delta f$.

Index	MF-DFA with $\ell = 1$				MF-DFA with $\ell = 2$			
	Δf	$\langle\Delta\hat{f}\rangle$	$\sigma_{\Delta\hat{f}}$	p -value	Δf	$\langle\Delta\hat{f}\rangle$	$\sigma_{\Delta\hat{f}}$	p -value
GOI	0.2780	0.1245	0.0724	0.0150	0.3819	0.1474	0.0601	0.0000
Wheat	0.1435	0.1977	0.0848	0.7660	0.3523	0.1885	0.0745	0.0140
Maize	0.2338	0.1665	0.0727	0.1680	0.1812	0.1649	0.0596	0.3880
Soyabeans	0.5991	0.1870	0.0711	0.0000	0.8569	0.2069	0.0597	0.0000
Rice	0.2182	0.3426	0.1603	0.7720	0.2431	0.3634	0.1476	0.7960
Barley	0.7493	0.4602	0.1190	0.0130	0.9276	0.4841	0.1066	0.0000

4. Summary and conclusion

We have performed multifractal detrended fluctuation analysis on six spot price indices of the global grain markets. To check if the extracted apparent multifractality is caused by the intrinsic nonlinear correlations in the original time series, we performed extensive statistical tests using surrogate time series generated by the IAAFT algorithm that preserve the values and power spectra of the original time series but destroy any nonlinear long-range correlations. We summarize and compare the MF-DMA and MF-DFA results of statistical tests for multifractal nature in Table 5. The column “ $dH(q)/dq < 0$ ” checks if $H(q)$ is a monotonically decreasing function. For a multifractal time series, we should have $dH(q)/dq < 0$. The column “Bell-shaped” checks if the singularity spectrum is bell-shaped without a knotted tie on the top. The singularity spectrum $f(\alpha)$ of a multifractal time series should be bell-shaped without a knotted tie. The column “ $a_2 \neq 0$ ” checks if $\tau(q)$ is a nonlinear function with $\Pr(a_2 \neq 0) < 0.05$. A multifractal time series should have a nonlinear $\tau(q)$ function so that $a_2 \neq 0$. The column of “ $a_2 < 0$ ” checks if the coefficient $a_2 < 0$. A multifractal time series should have a concave $\tau(q)$ function so that $a_2 < 0$. We would like to point out that these criteria are used to check if the time series exhibits apparent multifractality. The column “ $\Pr(\Delta\alpha < \Delta\hat{\alpha})$ ” shows the p -values of $\Delta\alpha < \Delta\hat{\alpha}$. For a multifractal time series, its singularity width $\Delta\alpha$ should be wider than the singularity width $\Delta\hat{\alpha}$ of its IAAFT surrogates. The column “ $\Pr(\Delta f < \Delta\hat{f})$ ” shows the p -values of $\Delta f < \Delta\hat{f}$. For a multifractal time series, we expect that its spectrum difference Δf should be greater than the spectrum difference $\Delta\hat{f}$ of its IAAFT surrogates. However, we note that it is also possible to have $\Delta f < \Delta\hat{f}$ for multifractal and non-multifractal time series. Hence, this last column is to provide further supporting evidence for the presence of multifractal nature in time series, but not to reject the presence of multifractality.

We find that, for the maize spot price index and all three methods (MF-DMA, MF-DFA with $\ell = 1$, and MF-DFA with $\ell = 2$), the generalized Hurst index functions $H(q)$ are monotonically decreasing ($dH(q)/dq < 0$), the singularity spectra $f(\alpha)$ are concave and bell-shaped, and the mass exponent functions $\tau(q)$ are nonlinear and concave. Moreover, all the three p -values of $\Delta\alpha < \Delta\hat{\alpha}$ are less than 5%. Therefore, the maize spot price index exhibits an undoubted intrinsic multifractal nature. For the barley spot price index, the generalized Hurst index functions $H(q)$ are monotonically decreasing ($dH(q)/dq < 0$), the singularity spectra $f(\alpha)$ are concave and bell-shaped, and the mass exponent functions $\tau(q)$ are nonlinear and concave. we argue that there is also an intrinsic multifractal nature, which is supported by all the information except that the p -value of $\Delta\alpha < \Delta\hat{\alpha}$ is 0.0970 when the MF-DMA method is utilized. For the GOI and the soyabeans sub-index, MF-DMA denies the possible presence of apparent multifractality since $H(q)$ is not a monotonically decreasing function and $f(\alpha)$ is not bell-shaped. MF-DMA also denies the presence of intrinsic multifractality since the p -values of $\Delta\alpha < \Delta\hat{\alpha}$ is large. However, MF-DFA with $\ell = 1$ and MF-DFA with $\ell = 2$ support the presence of an intrinsic multifractal nature with high probability. For the wheat spot price index, MF-DMA and MF-DFA with $\ell = 1$ deny the possible presence of apparent multifractality due to the incorrect shapes of $H(q)$ and $f(\alpha)$ and intrinsic multifractality due to the large p -values of $\Delta\alpha < \Delta\hat{\alpha}$. However, the results obtained

Table 5: Summary of the results of statistical tests for multifractal nature. The column of “ $dH(q)/dq$ ” checks if $H(q)$ is a monotonically decreasing function. The column of “Bell-shaped” checks if the singularity spectrum is bell-shaped without a knotted tie on the top. The column of “ $a_2 \neq 0$ ” checks if $\tau(q)$ is a nonlinear function with $\Pr(a_2 \neq 0) < 0.05$. The column of “ $a_2 < 0$ ” checks if the coefficient $a_2 < 0$. The column of “ $\Pr(\Delta\alpha < \Delta\hat{\alpha})$ ” shows the p -values of $\Delta\alpha < \Delta\hat{\alpha}$. The column of “ $\Pr(\Delta f < \Delta\hat{f})$ ” shows the p -values of $\Delta f < \Delta\hat{f}$.

Index	Method	$dH(q)/dq < 0$	Bell-shaped	$a_2 \neq 0$	$a_2 < 0$	$\Pr(\Delta\alpha < \Delta\hat{\alpha})$	$\Pr(\Delta f < \Delta\hat{f})$
Maize	MF-DMA	✓	✓	✓	✓	0.0010	0.0010
	MF-DFA ($\ell = 1$)	✓	✓	✓	✓	0.0040	0.1680
	MF-DFA ($\ell = 2$)	✓	✓	✓	✓	0.0310	0.3880
Barley	MF-DMA	✓	✓	✓	✓	0.0970	0.0690
	MF-DFA ($\ell = 1$)	✓	✓	✓	✓	0.0200	0.0130
	MF-DFA ($\ell = 2$)	✓	✓	✓	✓	0.0010	0.0000
GOI	MF-DMA	✗	✗	✓	✗	0.7140	0.2040
	MF-DFA ($\ell = 1$)	✓	✓	✓	✓	0.0090	0.0150
	MF-DFA ($\ell = 2$)	✓	✓	✓	✓	0.0000	0.0000
Soyabeans	MF-DMA	✗	✗	✓	✓	0.2110	0.0380
	MF-DFA ($\ell = 1$)	✓	✓	✓	✓	0.0000	0.0000
	MF-DFA ($\ell = 2$)	✓	✓	✓	✓	0.0000	0.0000
Wheat	MF-DMA	✗	✗	✗	✗	0.8970	0.6770
	MF-DFA ($\ell = 1$)	✗	✗	✓	✓	0.9040	0.7660
	MF-DFA ($\ell = 2$)	✓	✓	✓	✓	0.0640	0.0140
Rice	MF-DMA	✓	✓	✓	✓	0.6740	0.4020
	MF-DFA ($\ell = 1$)	✗	✗	✓	✗	1.0000	0.7720
	MF-DFA ($\ell = 2$)	✗	✗	✓	✓	0.9320	0.7960

by using MF-DFA with $\ell = 2$ show that the generalized Hurst index functions $H(q)$ are monotonically decreasing ($dH(q)/dq < 0$), the singularity spectra $f(\alpha)$ are concave and bell-shaped, and the mass exponent functions $\tau(q)$ are nonlinear and concave, which favors the possibility that there is intrinsic multifractality at the significance level of 0.0640. Finally, the rice spot price index suffers the most convincing evidence for the absence of an intrinsic multifractal nature. Particularly, the three p -values of $\Delta\alpha < \Delta\hat{\alpha}$ are all very large. Moreover, MF-DFA with $\ell = 1$ and MF-DFA with $\ell = 2$ suggest that there is even no apparent multifractality because $H(q)$ is not monotonically decreasing and $f(\alpha)$ is not bell-shaped (not concave).

The summarized results in Table 5 highlight the very complex nonlinear behavior of the global grain spot markets. Previous studies on other markets often reported the presence of multifractality, although many of them did not perform rigorous statistical tests [1]. On the one hand, we argue that, as what has been done in this work and in Ref. [16], any multifractal analysis of time series should perform similar statistical tests to confirm or deny the presence of multifractality. On the other hand, it is of vital importance to understand the underlying internal and external mechanisms that generate the multifractal or non-multifractal nature.

We note that, although the IAAFT technique is widely applied in nonlinear time series analysis, its asymptotic properties about statistical size and power (and hence consistency) have not been properly established. Theoretical and simulation studies reported that, in the context of IAAFT surrogates, the critical values used (or, equivalently, the p -values calculated) might not be appropriate [69–73]. As an alternative to the IAAFT method, the statically transformed autoregressive process (STAP) method was proposed [70, 74], which was found to give consistently good results in terms of the size and power of the test [73]. Therefore, it would be necessary to apply the STAP surrogates to check if the IAAFT algorithm over-rejects the null hypothesis of the absence of multifractality.

Acknowledgments

This work was partly supported by the National Natural Science Foundation of China (72171083), the Shanghai Outstanding Academic Leaders Plan, and the Fundamental Research Funds for the Central Universities.

References

- [1] Z.-Q. Jiang, W.-J. Xie, W.-X. Zhou, D. Sornette, Multifractal analysis of financial markets: a review, *Rep. Prog. Phys.* 82 (12) (2019) 125901. doi:10.1088/1361-6633/ab42fb.
- [2] L.-Y. He, S.-P. Chen, Are developed and emerging agricultural futures markets multifractal? a comparative perspective, *Physica A* 389 (18) (2010) 3828–3836. doi:10.1016/j.physa.2010.05.021.
- [3] L.-Y. He, S.-P. Chen, Multifractal detrended cross-correlation analysis of agricultural futures markets, *Chaos Solitons & Fractals* 44 (6) (2011) 355–361. doi:10.1016/j.chaos.2010.11.005.
- [4] Q. Wang, Y. Hu, Cross-correlation between interest rates and commodity prices, *Physica A* 428 (2015) 80–89. doi:10.1016/j.physa.2015.02.053.
- [5] H.-Y. Wang, Y.-S. Feng, Multivariate correlation analysis of agricultural futures and spot markets based on multifractal statistical methods, *J. Stat. Mech.* 2020 (7) (2020) 073403. doi:10.1088/1742-5468/ab900f.
- [6] T. Yin, Y. Wang, Nonlinear analysis and prediction of soybean futures, *Agric. Econ. Czech* 67 (5) (2021) 200–207. doi:10.17221/480/2020-AGRICECON.
- [7] S.-P. Chen, L.-Y. He, Multifractal spectrum analysis of nonlinear dynamical mechanisms in China's agricultural futures markets, *Physica A* 389 (7) (2010) 1434–1444. doi:10.1016/j.physa.2009.12.009.
- [8] Z. Li, X. Lu, Cross-correlations between agricultural commodity futures markets in the US and China, *Physica A* 391 (15) (2012) 3930–3941. doi:10.1016/j.physa.2012.02.029.
- [9] L.-Y. He, S.-P. Chen, Nonlinear bivariate dependency of price-volume relationships in agricultural commodity futures markets a perspective from multifractal detrended cross-correlation analysis, *Physica A* 390 (2) (2011) 297–308. doi:10.1016/j.physa.2010.09.018.
- [10] H. Kim, G. Oh, S. Kim, Multifractal analysis of the Korean agricultural market, *Physica A* 390 (23-24) (2011) 4286–4292. doi:10.1016/j.physa.2011.06.046.
- [11] L. Liu, Cross-correlations between crude oil and agricultural commodity markets, *Physica A* 395 (2014) 293–302. doi:10.1016/j.physa.2013.10.021.
- [12] F. Delbianco, F. Tohme, T. Stosic, B. Stosic, Multifractal behavior of commodity markets: fuel versus non-fuel products, *Physica A* 457 (2016) 573–580. doi:10.1016/j.physa.2016.03.096.
- [13] T. Stosic, S. A. Nejad, B. Stosic, Multifractal analysis of Brazilian agricultural market, *Fractals* 28 (5) (2020) 2050076. doi:10.1142/S0218348X20500760.
- [14] Y.-S. Feng, B.-M. Cao, Multifractal fluctuation analysis of correlations between agricultural futures markets in China and the US based on MF-X-DFA and MF-DPXA methods, *Fluctuation and Noise Letters* 21 (01) (2022) 2250006. doi:10.1142/S0219477522500067.
- [15] J. Wang, W. Shao, J. Kim, Analysis of the impact of COVID-19 on the correlations between crude oil and agricultural futures, *Chaos Solitons Fractals* 136 (2020) 109896. doi:10.1016/j.chaos.2020.109896.
- [16] X.-L. Gao, Y.-H. Shao, Y.-H. Yang, W.-X. Zhou, Do the global grain spot markets exhibit multifractal nature?, *Chaos Solitons Fractals* 164 (2022) 112663. doi:10.1016/j.chaos.2022.112663.
- [17] K. Matia, Y. Ashkenazy, H. E. Stanley, Multifractal properties of price fluctuations of stock and commodities, *EPL (Europhys. Lett.)* 61 (3) (2003) 422–428. doi:10.1209/epl/i2003-00194-y.
- [18] P. Oświęcimka, J. Kwapien, S. Drożdż, R. Rak, Investigating multifractality of stock market fluctuations using wavelet and detrending fluctuation methods, *Acta Phys. Pol. B* 36 (8) (2005) 2447–2457.
- [19] K. E. Lee, J. W. Lee, Origin of the multifractality of the Korean stock-market index, *J. Korean Phys. Soc.* 47 (2) (2005) 185–188.
- [20] J. Kwapien, P. Oświęcimka, S. Drożdż, Components of multifractality in high-frequency stock returns, *Physica A* 350 (2-4) (2005) 466–474. doi:10.1016/j.physa.2004.11.019.
- [21] S. Kumar, N. Deo, Multifractal properties of the Indian financial market, *Physica A* 388 (8) (2009) 1593–1602. doi:10.1016/j.physa.2008.12.017.
- [22] J. de Souza, S. M. D. Queirós, Effective multifractal features of high-frequency price fluctuations time series and ℓ -variability diagrams, *Chaos Solitons Fractals* 42 (4) (2009) 2512–2521. doi:10.1016/j.chaos.2009.03.198.
- [23] J. Theiler, S. Eubank, A. Longtin, B. Galdrikian, J. D. Farmer, Testing for nonlinearity in time series: The method of surrogate data, *Physica D* 58 (1992) 77–94. doi:10.1016/0167-2789(92)90102-S.
- [24] Q. Ruan, Z. Wang, J. Liu, D. Lv, Is foreign capital smarter? multifractal evidence from the Shanghai-Hong Kong stock connect program, *Fluct. Noise Lett.* 19 (4) (2020) 2050047. doi:10.1142/S0219477520500479.
- [25] Y.-S. Feng, H.-Y. Wang, Multifractal fluctuation analysis of correlations between the sector stock markets in China and the US, *Fluct. Noise Lett.* 20 (04) (2021) 2150031. doi:10.1142/S0219477521500310.
- [26] R. Zhao, P.-F. Dai, A multifractal cross-correlation analysis of economic policy uncertainty: evidence from China and US, *Fluct. Noise Lett.* 20 (05) (2021) 2150041. doi:10.1142/S0219477521500413.
- [27] W.-X. Zhou, The components of empirical multifractality in financial returns, *EPL* 88 (2) (2009) 28004. doi:10.1209/0295-5075/88/28004.
- [28] S. Drożdż, J. Kwapien, P. Oświęcimka, R. Rak, Quantitative features of multifractal subtleties in time series, *EPL (Europhys. Lett.)* 88 (6) (2009) 60003. doi:10.1209/0295-5075/88/60003.
- [29] W.-X. Zhou, Finite-size effect and the components of multifractality in financial volatility, *Chaos Solitons Fractals* 45 (2) (2012) 147–155. doi:10.1016/j.chaos.2011.11.004.

- [30] M. I. Bogachev, J. F. Eichner, A. Bunde, Effect of nonlinear correlations on the statistics of return intervals in multifractal data sets, *Phys. Rev. Lett.* 99 (24) (2007) 240601. doi:10.1103/PhysRevLett.99.240601.
- [31] J. Kwapien, P. Blasiak, S. Drozd, P. Oswiecimka, Genuine multifractality in time series is due to temporal correlations, *Phys. Rev. E* 107 (3) (2023) 034139.
- [32] T. Schreiber, A. Schmitz, Improved surrogate data for nonlinearity tests, *Phys. Rev. Lett.* 77 (4) (1996) 635–638. doi:10.1103/PhysRevLett.77.635.
- [33] T. Schreiber, A. Schmitz, Surrogate time series, *Physica D* 142 (3–4) (2000) 346–382. doi:10.1016/S0167-2789(00)00043-9.
- [34] P. Oswiecimka, S. Drozd, M. Frasca, R. Gębarowski, N. Yoshimura, L. Zunino, L. Minati, Wavelet-based discrimination of isolated singularities masquerading as multifractals in detrended fluctuation analyses, *Nonlinear Dyn.* 100 (2) (2020) 1689–1704. doi:10.1007/s11071-020-05581-y.
- [35] J. W. Kantelhardt, S. A. Zschiegner, E. Koscielny-Bunde, S. Havlin, A. Bunde, H. E. Stanley, Multifractal detrended fluctuation analysis of nonstationary time series, *Physica A* 316 (1–4) (2002) 87–114. doi:10.1016/S0378-4371(02)01383-3.
- [36] G.-F. Gu, W.-X. Zhou, Detrending moving average algorithm for multifractals, *Phys. Rev. E* 82 (1) (2010) 011136. doi:10.1103/PhysRevE.82.011136.
- [37] E. Alessio, A. Carbone, G. Castelli, V. Frappietro, Second-order moving average and scaling of stochastic time series, *Eur. Phys. J. B* 27 (2) (2002) 197–200. doi:10.1140/epjb/e20020150.
- [38] A. Carbone, G. Castelli, H. E. Stanley, Time-dependent Hurst exponent in financial time series, *Physica A* 344 (1–2) (2004) 267–271. doi:10.1016/j.physa.2004.06.130.
- [39] P. Grassberger, Generalized dimensions of strange attractors, *Phys. Lett. A* 97 (6) (1983) 227–230. doi:10.1016/0375-9601(83)90753-3.
- [40] P. Grassberger, I. Procaccia, Measuring the strangeness of strange attractors, *Physica D* 9 (1–2) (1983) 189–208. doi:10.1016/0167-2789(83)90298-1.
- [41] P. Grassberger, Generalizations of the Hausdorff dimension of fractal measure, *Phys. Lett. A* 107 (3) (1985) 101–105. doi:10.1016/0375-9601(85)90724-8.
- [42] A. N. Kolmogorov, A refinement of previous hypotheses concerning the local structure of turbulence in a viscous incompressible fluid at high Reynolds number, *J. Fluid Mech.* 13 (1) (1962) 82–85. doi:10.1017/S0022112062000518.
- [43] C. W. Van Atta, W. Y. Chen, Structure functions of turbulence in the atmospheric boundary layer over the ocean, *J. Fluid Mech.* 44 (1) (1970) 145–159. doi:10.1017/S002211207000174X.
- [44] T. Di Matteo, Multi-scaling in finance, *Quant. Financ.* 7 (1) (2007) 21–36. doi:10.1080/14697680600969727.
- [45] A. Arneodo, G. Grasseau, M. Holschneider, Wavelet transform of multifractals, *Phys. Rev. Lett.* 61 (20) (1988) 2281–2284. doi:10.1103/PhysRevLett.61.2281.
- [46] C. Carrizales-Velazquez, R. V. Donner, L. Guzman-Vargas, Generalization of Higuchi’s fractal dimension for multifractal analysis of time series with limited length, *Nonlinear Dyn.* 108 (1) (2022) 417–431. doi:10.1007/s11071-022-07202-2.
- [47] X.-Y. Qian, G.-F. Gu, W.-X. Zhou, Modified detrended fluctuation analysis based on empirical mode decomposition for the characterization of anti-persistent processes, *Physica A* 390 (23–24) (2011) 4388–4395. doi:10.1016/j.physa.2011.07.008.
- [48] J. Lin, C. Dou, Y. Liu, Multifractal detrended fluctuation analysis based on optimized empirical mode decomposition for complex signal analysis, *Nonlinear Dyn.* 103 (3) (2021) 2461–2474. doi:10.1007/s11071-021-06223-7.
- [49] R. D. Urda-Benitez, A. E. Castro-Ospina, A. Orozco-Duque, Characterization and classification of intracardiac atrial fibrillation signals using the time-singularity multifractal spectrum distribution, *Commun. Nonlinear Sci. Numer. Simul.* 96 (2021) 105675. doi:10.1016/j.cnsns.2020.105675.
- [50] D. Nian, Z. Fu, Extended self-similarity based multi-fractal detrended fluctuation analysis: A novel multi-fractal quantifying method, *Commun. Nonlinear Sci. Numer. Simul.* 67 (2019) 568–576. doi:10.1016/j.cnsns.2018.07.034.
- [51] C.-K. Peng, S. V. Buldyrev, S. Havlin, M. Simons, H. E. Stanley, A. L. Goldberger, Mosaic organization of DNA nucleotides, *Phys. Rev. E* 49 (2) (1994) 1685–1689. doi:10.1103/PhysRevE.49.1685.
- [52] A. Castro e Silva, J. G. Moreira, Roughness exponents to calculate multi-affine fractal exponents, *Physica A* 235 (3) (1997) 327–333. doi:10.1016/S0378-4371(96)00357-3.
- [53] R. O. Weber, P. Talkner, Spectra and correlations of climate data from days to decades, *J. Geophys. Res.* 106 (2001) 20131–20144. doi:10.1029/2001GL014170.
- [54] D. Headey, Rethinking the global food crisis: the role of trade shocks, *Food Policy* 36 (2) (2011) 136–146. doi:10.1016/j.foodpol.2010.10.003.
- [55] P. C. Abbott, Export restrictions as stabilization responses to food crisis, *Am. J. Agr. Econ.* 94 (2) (2012) 428–434. doi:10.1093/ajae/aar092.
- [56] A. Bouet, D. L. Debucquet, Food crisis and export taxation: the cost of non-cooperative trade policies, *Rev. World Econ.* 148 (1) (2012) 209–233. doi:10.1007/s10290-011-0108-8.
- [57] C. B. Barrett, Actions now can curb food systems fallout from COVID-19, *Nat. Food* 1 (6) (2020) 319–320. doi:10.1038/s43016-020-0085-y.
- [58] S. Akter, The impact of COVID-19 related ‘stay-at-home’ restrictions on food prices in Europe: findings from a preliminary analysis, *Food Secur.* 12 (4) (2020) 719–725. doi:10.1007/s12571-020-01082-3.
- [59] T. Falkendal, C. Otto, J. Schewe, J. Jagermeyr, M. Konar, M. Kumm, B. Watkins, M. J. Puma, Grain export restrictions during COVID-19 risk food insecurity in many low- and middle-income countries, *Nat. Food* 2 (1) (2021) 11–14. doi:10.1038/s43016-020-00211-7.
- [60] L.-J. Ji, W.-X. Zhou, H.-F. Liu, X. Gong, F.-C. Wang, Z.-H. Yu, R/S method for unevenly sampled time series: application to detecting long-term temporal dependence of droplets transiting through a fixed spatial point in gas-liquid two-phase turbulent jets, *Physica A* 388 (17) (2009) 3345–3354. doi:10.1016/j.physa.2009.05.006.
- [61] P. Oswiecimka, S. Drozd, J. Kwapien, A. Z. Gorski, Effect of detrending on multifractal characteristics, *Acta Phys. Pol. A* 123 (3) (2013) 597–603. doi:10.12693/APhysPolA.123.597.

- [62] V. S. L'vov, E. Podivilov, A. Pomyalov, I. Procaccia, D. Vandembroucq, Improved shell model of turbulence, *Phys. Rev. E* 58 (2) (1998) 1811–1822. doi:10.1103/PhysRevE.58.1811.
- [63] W.-X. Zhou, D. Sornette, W.-K. Yuan, Inverse statistics and multifractality of exit distances in 3D fully developed turbulence, *Physica D* 214 (1) (2006) 55–62. doi:10.1016/j.physd.2005.12.004.
- [64] O. Malcai, D. A. Lidar, O. Biham, D. Avnir, Scaling range and cutoffs in empirical fractals, *Phys. Rev. E* 56 (3) (1997) 2817–2828. doi:10.1103/PhysRevE.56.2817.
- [65] D. Avnir, O. Biham, D. Lidar, O. Malcai, Is the geometry of nature fractal?, *Science* 279 (5347) (1998) 39–40. doi:10.1126/science.279.5347.39.
- [66] D. Sornette, Discrete scale invariance and complex dimensions, *Phys. Rep.* 297 (5) (1998) 239–270, extended version at <https://arxiv.org/abs/cond-mat/9707012>. doi:10.1016/S0370-1573(97)00076-8.
- [67] Z.-Q. Jiang, W.-X. Zhou, Multifractality in stock indexes: fact or fiction?, *Physica A* 387 (14) (2008) 3605–3614. doi:10.1016/j.physa.2008.02.015.
- [68] Z.-Q. Jiang, W.-X. Zhou, Multifractal analysis of Chinese stock volatilities based on the partition function approach, *Physica A* 387 (19–20) (2008) 4881–4888. doi:10.1016/j.physa.2008.04.028.
- [69] D. Kugiumtzis, Test your surrogate data before you test for nonlinearity, *Phys. Rev. E* 60 (3) (1999) 2808–2816. doi:10.1103/PhysRevE.60.2808.
- [70] D. Kugiumtzis, Surrogate data test for nonlinearity including nonmonotonic transforms, *Phys. Rev. E* 62 (1) (2000) R25–R28. doi:10.1103/PhysRevE.62.R25.
- [71] D. Kugiumtzis, On the reliability of the surrogate data test for nonlinearity in the analysis of noisy time series, *Int. J. Bifurcation Chaos* 11 (7) (2001) 1881–1896. doi:10.1142/S0218127401003061.
- [72] E. Mammen, S. Nandi, Change of the nature of a test when surrogate data are applied, *Phys. Rev. E* 70 (1) (2004) 016121. doi:10.1103/PhysRevE.70.016121.
- [73] D. Kugiumtzis, Evaluation of surrogate and bootstrap tests for nonlinearity in time series, *Stud. Nonlinear Dyn. Econom.* 12 (1) (2008) 4.
- [74] D. Kugiumtzis, Statically transformed autoregressive process and surrogate data test for nonlinearity, *Phys. Rev. E* 66 (2) (2002) 025201. doi:10.1103/PhysRevE.66.025201.

Appendix A. Comparison of MF-DFA results

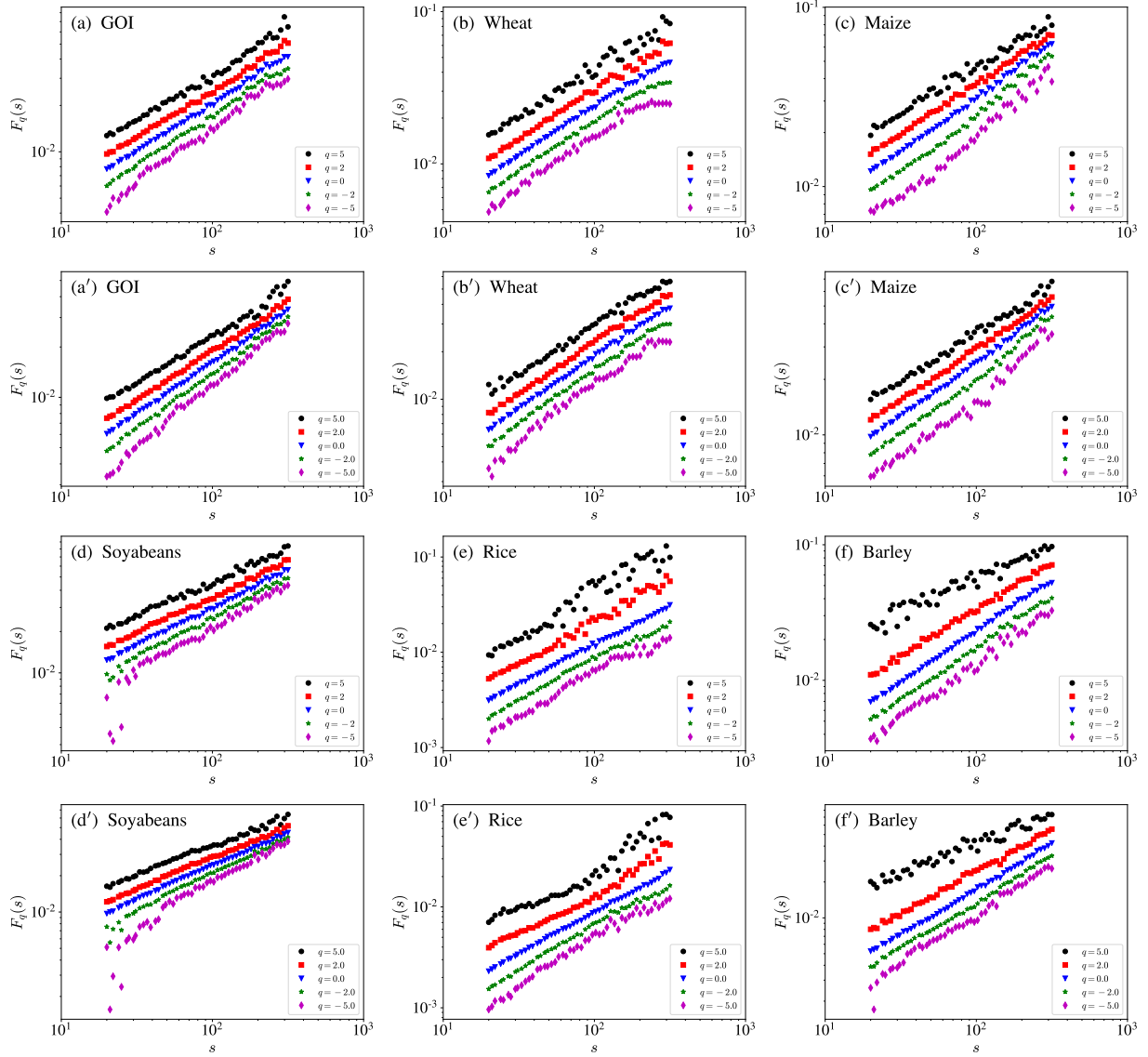


Figure A1: Scaling plots of the MF-DMA fluctuation function $F_q(s)$ with respect to the scale s for the GOI index [(a) for $\ell = 1$ and (a') for $\ell = 2$], the wheat sub-index [(b) for $\ell = 1$ and (b') for $\ell = 2$], the maize sub-index [(c) for $\ell = 1$ and (c') for $\ell = 2$], the soyabeans sub-index [(d) for $\ell = 1$ and (d') for $\ell = 2$], the rice sub-index [(e) for $\ell = 1$ and (e') for $\ell = 2$], and the barley sub-index [(f) for $\ell = 1$ and (f') for $\ell = 2$] released by the International Grains Council.

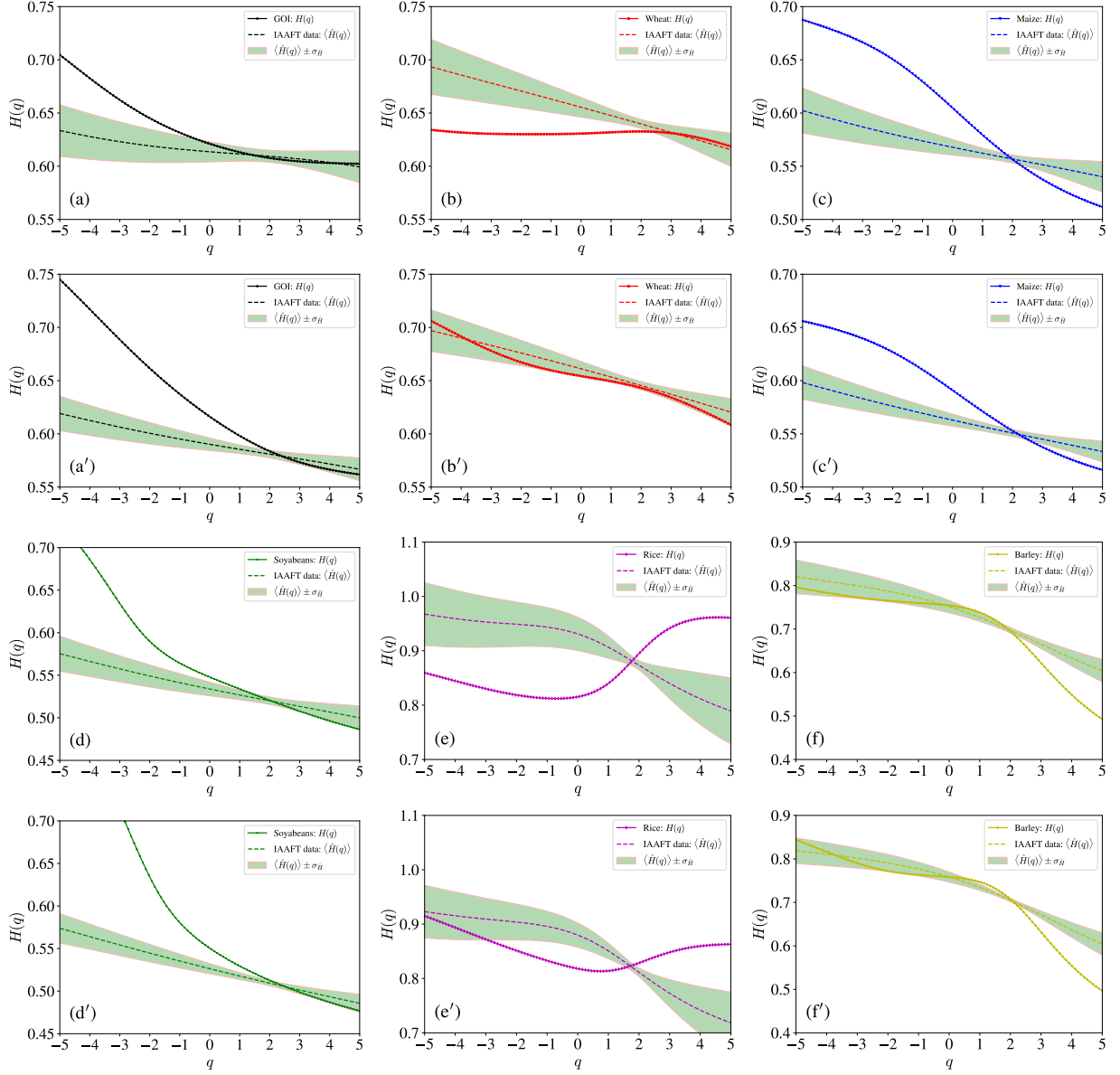


Figure A2: Generalized Hurst indexes $H(q)$ with respect to the order q for the GOI index [(a) for $\ell = 1$ and (a') for $\ell = 2$], the wheat sub-index [(b) for $\ell = 1$ and (b') for $\ell = 2$], the maize sub-index [(c) for $\ell = 1$ and (c') for $\ell = 2$], the soybeans sub-index [(d) for $\ell = 1$ and (d') for $\ell = 2$], the rice sub-index [(e) for $\ell = 1$ and (e') for $\ell = 2$], and the barley sub-index [(f) for $\ell = 1$ and (f') for $\ell = 2$] released by the International Grains Council. For each GOI and sub-indices, we generate 1000 surrogate time series using the IAAFT algorithm and calculate the mean $\langle \hat{H} \rangle$ and standard deviation $\sigma_{\hat{H}}$.

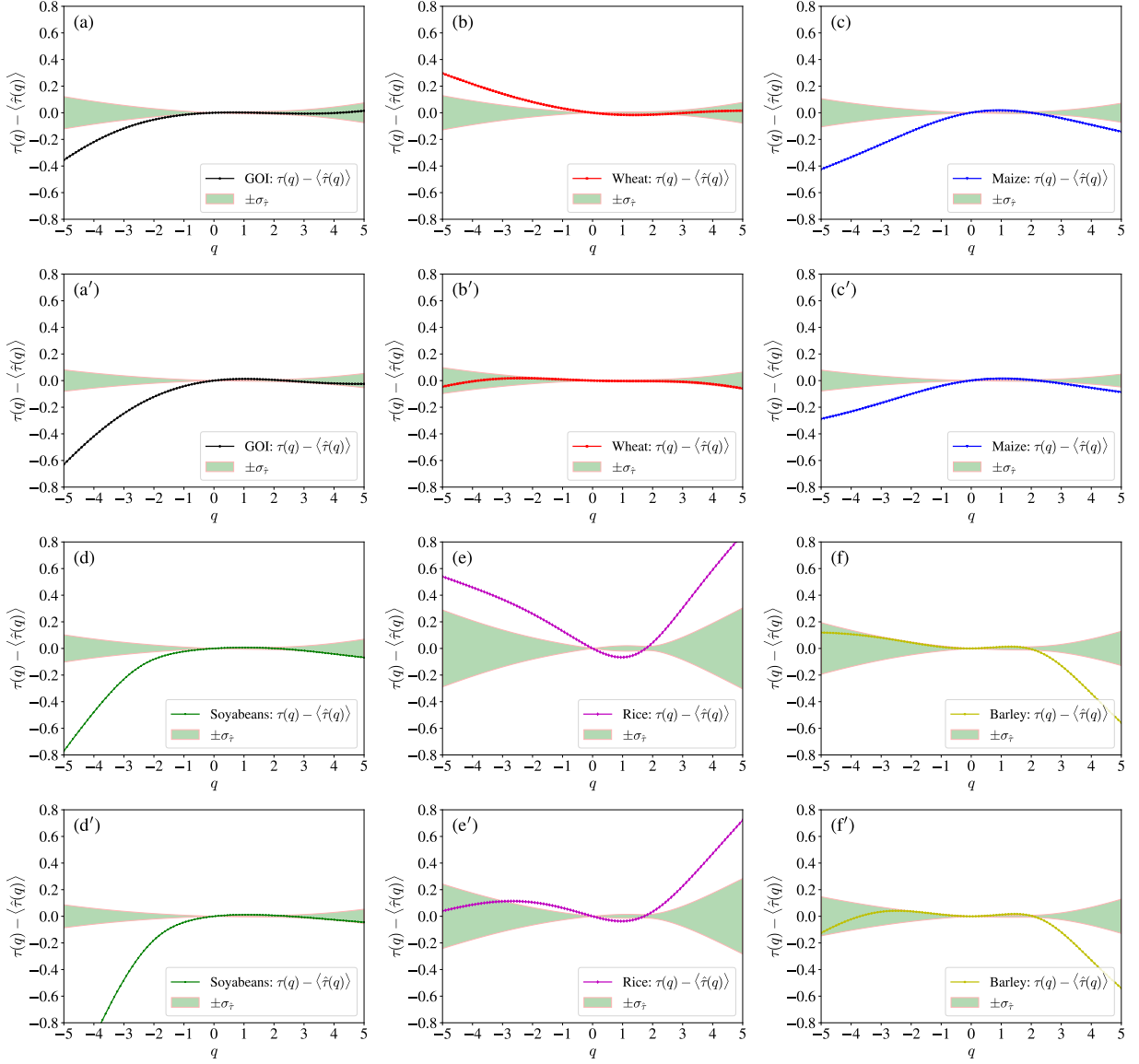


Figure A3: Deviations $(\tau(q) - \langle \hat{\tau}(q) \rangle)$ of the mass exponents $\tau(q)$ of the original time series from the average mass exponents $\langle \hat{\tau}(q) \rangle$ of the IAAFT surrogates with respect to the order q for the GOI index [(a) for $\ell = 1$ and (a') for $\ell = 2$], the wheat sub-index [(b) for $\ell = 1$ and (b') for $\ell = 2$], the maize sub-index [(c) for $\ell = 1$ and (c') for $\ell = 2$], the soyabeans sub-index [(d) for $\ell = 1$ and (d') for $\ell = 2$], the rice sub-index [(e) for $\ell = 1$ and (e') for $\ell = 2$], and the barley sub-index [(f) for $\ell = 1$ and (f') for $\ell = 2$] released by the International Grains Council. For each GOI and sub-indices, we generate 1000 surrogate time series using the IAAFT algorithm and calculate the mean $\langle \hat{\tau} \rangle$ and standard deviation $\sigma_{\hat{\tau}}$.

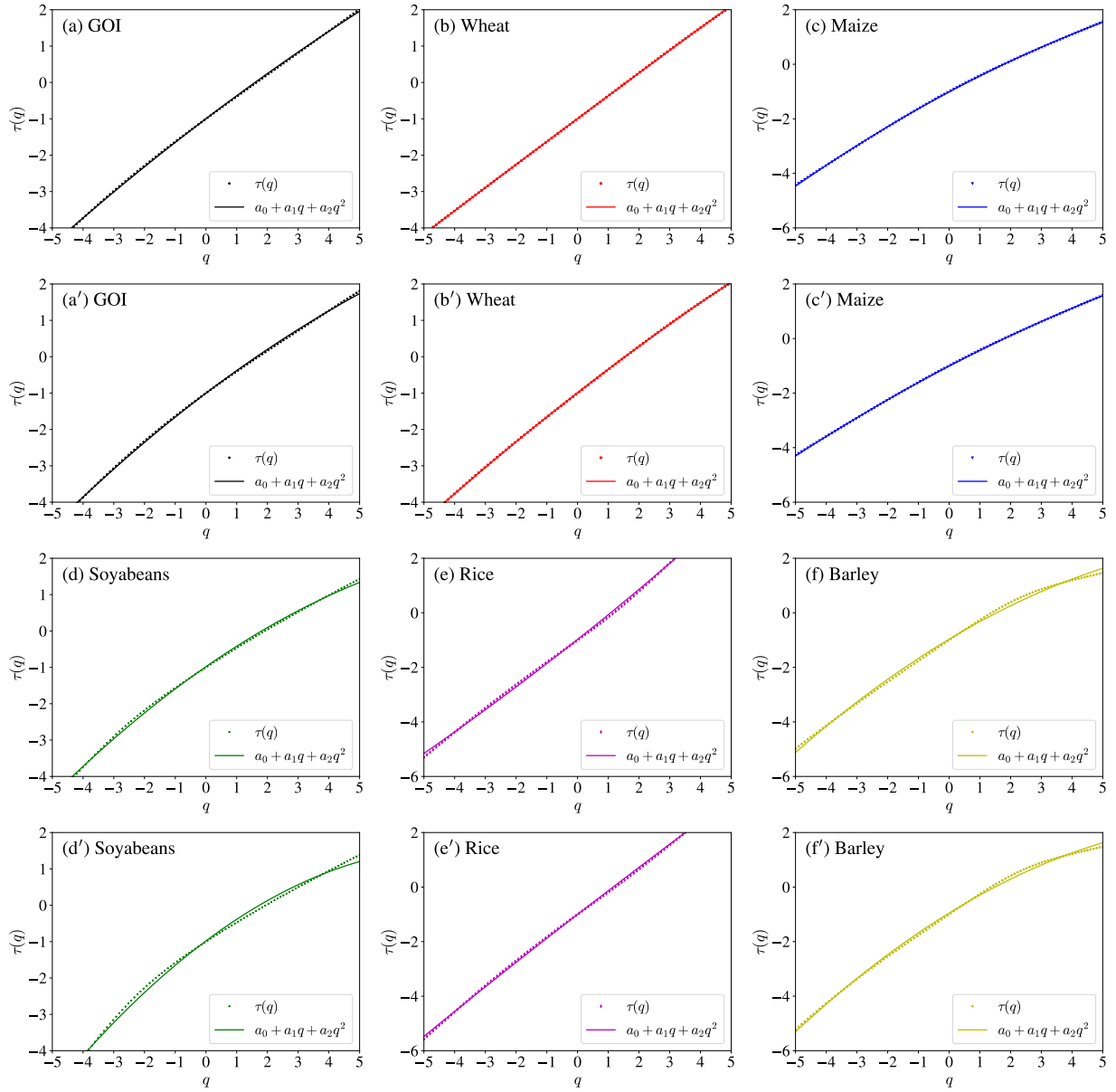


Figure A4: Testing the nonlinearity in the mass exponents $\tau(q)$ for the GOI index [(a) for $\ell = 1$ and (a') for $\ell = 2$], the wheat sub-index [(b) for $\ell = 1$ and (b') for $\ell = 2$], the maize sub-index [(c) for $\ell = 1$ and (c') for $\ell = 2$], the soyabeans sub-index [(d) for $\ell = 1$ and (d') for $\ell = 2$], the rice sub-index [(e) for $\ell = 1$ and (e') for $\ell = 2$], and the barley sub-index [(f) for $\ell = 1$ and (f') for $\ell = 2$].

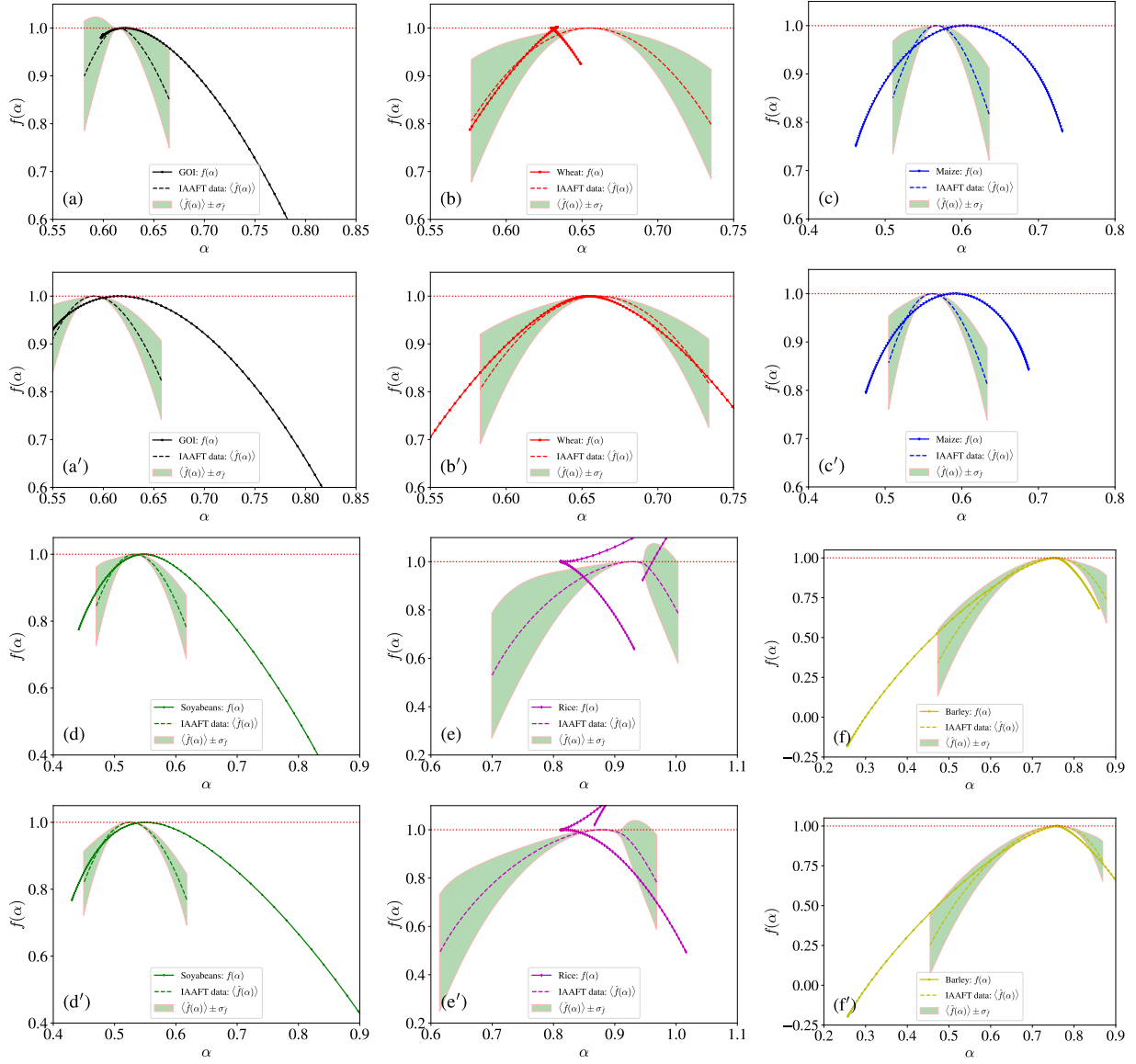


Figure A5: Singularity spectrum $f(\alpha)$ with respect to the singularity α for the GOI index [(a) for $\ell = 1$ and (a') for $\ell = 2$], the wheat sub-index [(b) for $\ell = 1$ and (b') for $\ell = 2$], the maize sub-index [(c) for $\ell = 1$ and (c') for $\ell = 2$], the soybeans sub-index [(d) for $\ell = 1$ and (d') for $\ell = 2$], the rice sub-index [(e) for $\ell = 1$ and (e') for $\ell = 2$], and the barley sub-index [(f) for $\ell = 1$ and (f') for $\ell = 2$] released by the International Grains Council. For each GOI and sub-indices, we generate 1000 surrogate time series using the IAAFT algorithm and calculate the mean $\langle \hat{f} \rangle(\alpha)$ and standard deviation $\sigma_{\hat{f}}$.

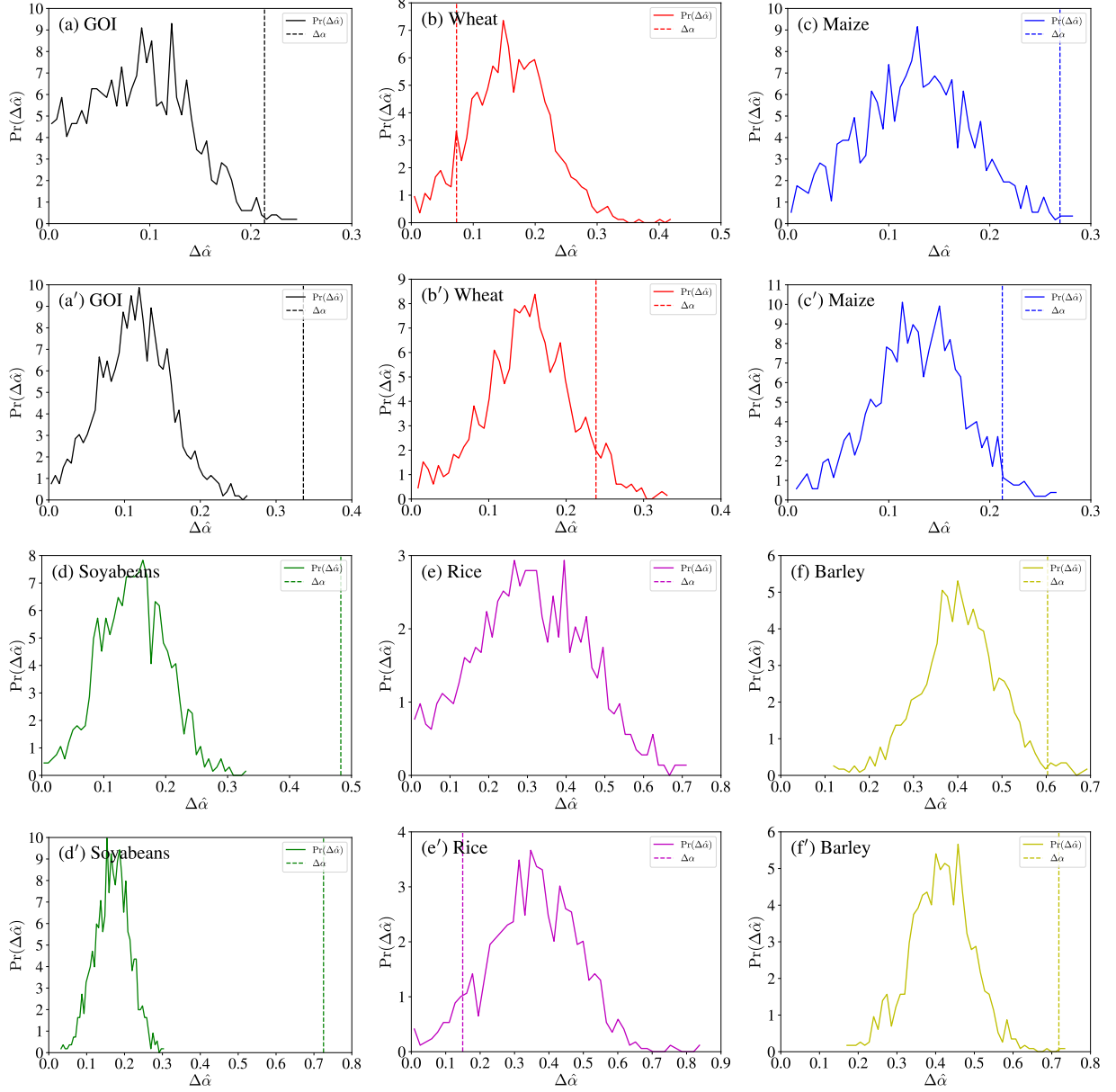


Figure A6: Empirical distribution of the singularity widths $\Delta\hat{\alpha}$ of the 1000 IAAFT surrogates for the GOI index [(a) for $\ell = 1$ and (a') for $\ell = 2$], the wheat sub-index [(b) for $\ell = 1$ and (b') for $\ell = 2$], the maize sub-index [(c) for $\ell = 1$ and (c') for $\ell = 2$], the soyabeans sub-index [(d) for $\ell = 1$ and (d') for $\ell = 2$], the rice sub-index [(e) for $\ell = 1$ and (e') for $\ell = 2$], and the barley sub-index [(f) for $\ell = 1$ and (f') for $\ell = 2$] released by the International Grains Council. The vertical dashed lines are the corresponding singularity widths $\Delta\alpha$ of the original time series.

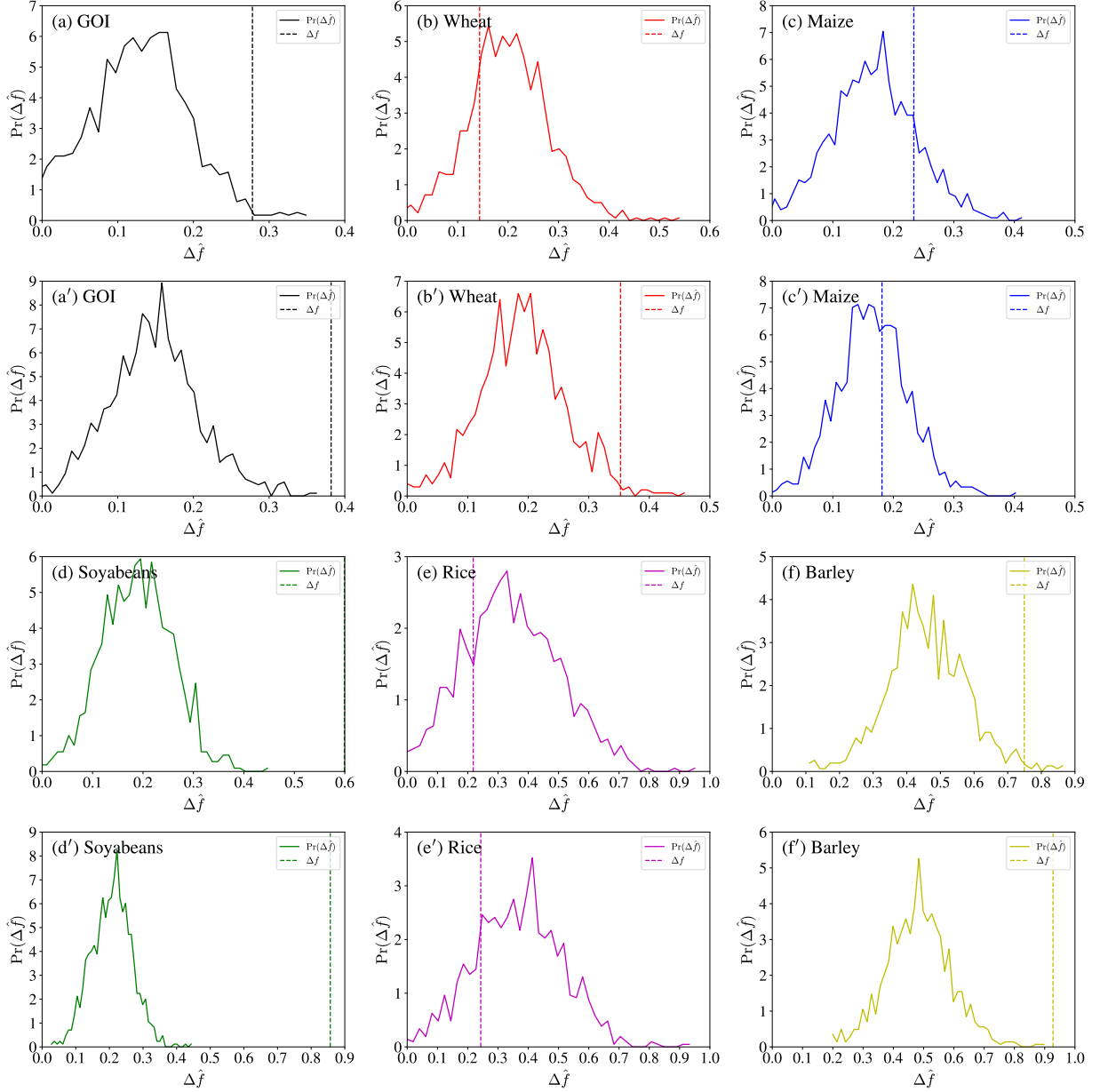


Figure A7: Empirical distribution of the spectrum differences $\Delta\hat{f}$ of the 1000 IAAFT surrogates for the GOI index [(a) for $\ell = 1$ and (a') for $\ell = 2$], the wheat sub-index [(b) for $\ell = 1$ and (b') for $\ell = 2$], the maize sub-index [(c) for $\ell = 1$ and (c') for $\ell = 2$], the soyabeans sub-index [(d) for $\ell = 1$ and (d') for $\ell = 2$], the rice sub-index [(e) for $\ell = 1$ and (e') for $\ell = 2$], and the barley sub-index [(f) for $\ell = 1$ and (f') for $\ell = 2$] released by the International Grains Council. The vertical dashed lines are the corresponding spectrum differences Δf of the original time series.